

A Comparison of the Coordination Behaviour of R₂PCH₂BMe₂ (R = Me vs Ph) Ambiphilic Ligands with Late Transition Metals

Katia M. Paskaruk, David J. H. Emslie,* and James F. Britten

Received 00th January 20xx,
Accepted 00th January 20xx

DOI: 10.1039/x0xx00000x

A new synthesis that avoids the use of Me₂PH is reported for (Me₂PCH₂BMe₂)₂, and this method was extended to the synthesis of (Ph₂PCH₂BMe₂)₂. The ligand precursor (Me₂PCH₂BMe₂)₂ did not react with [M(μ-Cl)(cod)]₂ (cod = 1,5-cyclooctadiene; M = Ir and Rh) or [PtCl₂(cod)] at room temperature. However, after 12–48 hours at 65–70 °C, these reactions afforded (a) [Ir(cod)(μ-Cl)(Me₂PCH₂BMe₂)] (1), (b) an equilibrium mixture of (Me₂PCH₂BMe₂)₂, [Rh(μ-Cl)(cod)]₂ and [Rh(cod)(μ-Cl)(Me₂PCH₂BMe₂)] (2), and (c) *cis*-[Pt(μ-Cl)₂(Me₂PCH₂BMe₂)₂] (3), respectively. By contrast, reactions between the phenyl-substituted analogue, (Ph₂PCH₂BMe₂)₂, and [M(μ-Cl)(cod)]₂ (cod = 1,5-cyclooctadiene; M = Rh and Ir) proceeded over the course of 1 hour at 20 °C to generate [M(cod)(μ-Cl)(Ph₂PCH₂BMe₂)] (M = Ir (4) and Rh (5)), indicative of room temperature (Ph₂PCH₂BMe₂)₂ dissociation. Room temperature reactions of (Ph₂PCH₂BMe₂)₂ with [Rh(μ-Cl)(coe)₂]₂ (coe = cyclooctene) using a 1:1 or 3:1 stoichiometry also afforded [Rh(coe)(μ-Cl)(Ph₂PCH₂BMe₂)₂] (6) and [RhCl(Ph₂PCH₂BMe₂)₃] (7), where the latter is a borane-appended analogue of Wilkinson's catalyst, and reactions of (Ph₂PCH₂BMe₂)₂ with [PtX₂(cod)] (X = Cl or Me) yielded *cis*-[Pt(μ-Cl)₂(Ph₂PCH₂BMe₂)₂] (8) and *cis*-[PtMe₂(Ph₂PCH₂BMe₂)₂] (9). Compounds 1–9, (Me₂PCH₂BMe₂)₂ and (Ph₂PCH₂BMe₂)₂ were crystallographically characterized. In compounds 1–5 and 8, each chloride co-ligand is coordinated by the borane of an R₂PCH₂BMe₂ ligand. Additionally, in the solid state structure of 6, each bridging chloride ligand interacts weakly with a pendent borane, and in 7, the chloride ligand is tightly coordinated to the borane of one Ph₂PCH₂BMe₂ ligand and weakly coordinated to the borane of a second Ph₂PCH₂BMe₂ ligand. By contrast, both boranes in 9 (and one of the three boranes in 7) are non-coordinated.

Introduction

Transition metal complexes bearing ambiphilic ligands are of particular interest due to the ability of the Lewis acid to influence the reactivity of the complex. This can occur through a variety of mechanisms, including modulation of electron density at the metal centre via direct metal–Lewis acid coordination, and interaction of the Lewis acid with co-ligands or incoming substrates, both of which have potential applications in cooperative catalysis.^{1,2}

To promote interactions with co-ligands and substrates, phosphine-borane ligands with a single atom bridging between phosphorus and boron may be beneficial, since chelation to form a metal–borane interaction will be disfavoured as a result of 4-membered ring formation. However, complexes bearing such ligands are scarce; examples are shown in Figure 1. Early work generated [MH(μ-H)(PMe₃)₃(Me₂PCH₂BR₂)] complexes (M = Ru or Os; BR₂ = 9-borabicyclononyl or BH(CMe₂/Pr)), in which one hydride ligand bridges between the metal and boron, via reactions of [MH(η²-CH₂PMe₂)(PMe₃)₃] with HBR₂.³ The chemistry of the Ph₂PCH₂BR₂ (BR₂ = 9-borabicyclononyl) ligand

was then extended to rhenium, including reactions of [Re(CO)₄(Ph₂PCH₂BR₂)₂]⁺ with 1 or 2 equiv. of [PtH(dmpe)₂]⁺ to form [Re(CO)₃(μ-CHO)(Ph₂PCH₂BR₂)₂] and [Re(CO)₃(μ-OCH₂BR₂CH₂PPh₂)(Ph₂PCH₂BR₂)₂][−], respectively (Figure 1).⁴ Rhodium complexes of Ph₂PCHMeBR₂ (BR₂ = 9-borabicyclononyl)⁵ and ¹Pr₂POB{(NH)₂C₁₀H₆}⁶ ligands have also been prepared, as have gold^{7,8} and/or copper⁹ complexes of ^tBu₂PCH₂BPh₂ and Ph₂PN(Dipp)BCy₂ ligands (Figure 1). The reaction of [AuCl(PPh₃)] with ^tBu₂PCH₂BPh₂ afforded zwitterionic [Au(^tBu₂PCH₂BPh₂Cl)(PPh₃)], and reaction of [AuCl(SMe₂)] with excess ^tBu₂PCH₂BPh₂ yielded [Au(^tBu₂PCH₂BPh₂Cl)(^tBu₂PCH₂BPh₂)]. In all other cases, interactions between the borane and the metal or co-ligands were not observed. [(dppf)Pt(μ-OH)(Me₂BOBAR^F₂)] {Ar^F = C₆H₃(CF₃)₂-3,5} was also recently reported, arising from the reaction of [(dppf)Pt(PMe₂OH)][OTf]₂ with 2 equiv. of K[BAR^F₄] in the presence of water.¹⁰ Additionally, tungsten complexes of a Ph₂PCH(BR₂)CH₂PPh₂ ligand (BR₂ = 9-borabicyclononyl) have been synthesized, with a 1-atom bridge between the borane and one of the two phosphines. These complexes include [Mn(CO)₂(μ-CHO){Ph₂PCH(BR₂)CH₂PPh₂}], in which the borane is coordinated to the oxygen atom of a formyl ligand.^{11,12} Furthermore, [Fe(η⁵-C₅H₄BMEnPhPPh₂)₂{Cr(CO)₅}₂] has been described, in which each phosphine donor is coordinated to a Cr(CO)₅ fragment.¹³

Herein we report the coordination chemistry of simple R₂PCH₂BMe₂ (R = Me, Ph) ligands with iridium, rhodium and

^a Department of Chemistry and Chemical Biology, McMaster University, Hamilton, Ontario L8S 4M1, Canada. E-mail: emslied@mcmaster.ca

Electronic Supplementary Information (ESI) available: NMR spectra, and crystallographic and computational details. See DOI: 10.1039/x0xx00000x. CCDC 2282160–2282170 for Me₂PCH₂BMe₂, 1, 2, [Rh(μ-Cl)(cod)]₂, 3, Ph₂PCH₂BMe₂, 4–0.5 CH₂Cl₂, 5–CH₂Cl₂, 6–2 CH₂Cl₂, and 7–9, respectively.

platinum. The transition metal chemistry of these ligands has not previously been investigated, and a notable feature of the ligands (in addition to the 1-atom linker between phosphorus and boron) is the low steric requirement of the substituents on boron; most other ambiphilic ligands with hydrocarbyl substituents on boron employ aryl (e.g. $\text{BR}_2 = \text{BPh}_2$ or BMe_2) or bulky alkyl (e.g. $\text{BR}_2 = \text{BCy}_2$ or 9-borabicyclononyl) groups.¹

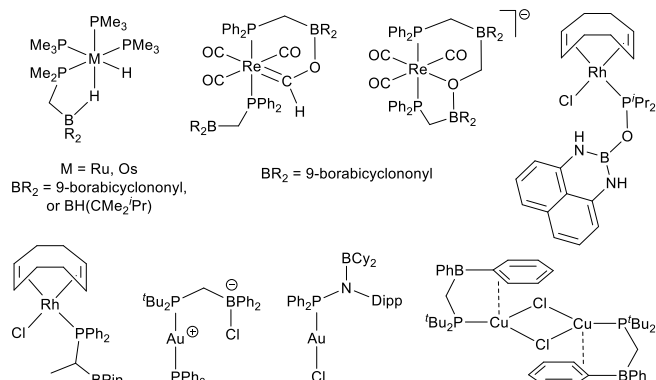
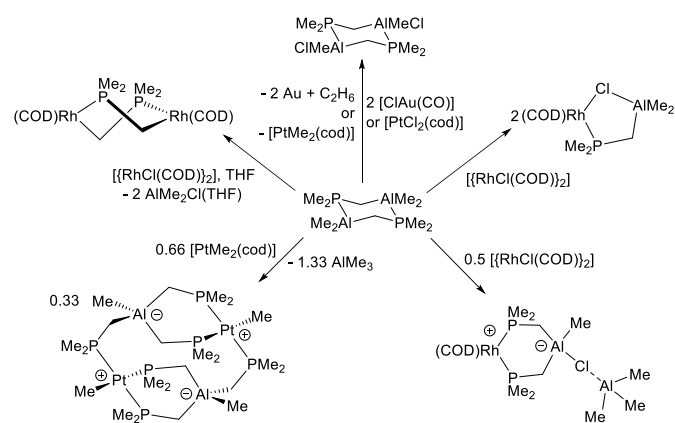


Figure 1. Examples of transition metal complexes bearing phosphine-borane ambiphilic ligands with a 1-atom linker between phosphorus and boron (Dipp = 2,6- $\text{C}_6\text{H}_3\text{Pr}_2$).

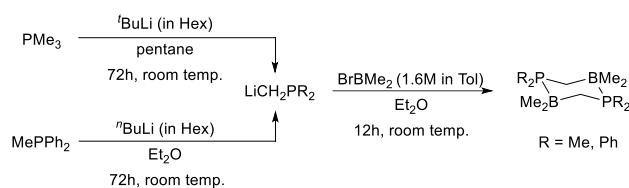
This work builds from our recent study of the coordination behaviour of $\text{Me}_2\text{PCH}_2\text{AlMe}_2$ ligands, which led to five distinct outcomes, all but one involving cleavage of Al–C bonds: (1) complexation of an intact $\text{Me}_2\text{PCH}_2\text{AlMe}_2$ ligand, (2) generation of a bis(phosphino)aluminate ligand, (3) generation of a tris(phosphino)aluminate ligand, (4) formation of a dimethylphosphinomethyl complex, and (5) chloride-methyl exchange to afford free $(\text{Me}_2\text{PCH}_2\text{AlClMe})_2$ (Scheme 1).¹⁴ The reactivity of $(\text{Me}_2\text{PCH}_2\text{AlMe}_2)_2$ with transition metal complexes has also been explored by the Zargarian¹⁵ and Fontaine groups,^{16,17} in some cases affording products resulting from Al–C bond cleavage. In the current work with boron analogues, B–C bond cleavage was not observed.



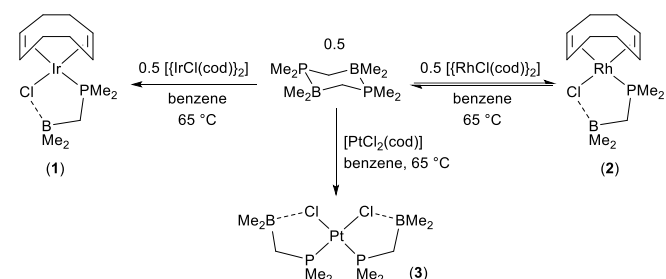
Scheme 1. Selected reactivity of $(\text{Me}_2\text{PCH}_2\text{AlMe}_2)_2$ with transition metal precursors.¹⁴

Results and Discussion

The ligand precursor $(\text{Me}_2\text{PCH}_2\text{BMe}_2)_2$ was first reported in 1971 by Schaeffer et al.,¹⁸ and was synthesized via the reaction of gaseous Me_2PH with $\text{Me}_2\text{BCH}_2\text{Cl}$ at 100 °C. However, to avoid the synthesis and handling of these reagents, we developed an alternative synthesis of $(\text{Me}_2\text{PCH}_2\text{BMe}_2)_2$, via the addition of a toluene solution of Me_2BBr to a suspension of $\text{LiCH}_2\text{PMe}_2$ in diethyl ether (Scheme 2). This synthesis is analogous to the method reported by Karsch for the preparation of $(\text{Me}_2\text{PCH}_2\text{AlMe}_2)_2$,¹⁹ and pure $(\text{Me}_2\text{PCH}_2\text{BMe}_2)_2$ was isolated in 50% yield by sublimation from the crude reaction mixture at 90 °C.



Scheme 2. Synthesis of $(\text{R}_2\text{PCH}_2\text{BMe}_2)_2$ (R = Me and Ph).



Scheme 3. Reactions of $(\text{Me}_2\text{PCH}_2\text{BMe}_2)_2$ to form complexes 1–3.

The coordination chemistry of $(\text{Me}_2\text{PCH}_2\text{BMe}_2)_2$ was examined with a variety of late transition metal precursors, including $\{[\text{M}(\mu\text{-Cl})(\text{cod})]_2\}$ (cod = 1,5-cyclooctadiene; M = Ir, Rh) and $[\text{PtX}_2(\text{cod})]$ (X = Me, Cl). All of these reactions failed to proceed at room temperature, presumably due a lack of dissociation of the $(\text{Me}_2\text{PCH}_2\text{BMe}_2)_2$ dimer; consistent with this hypothesis, the $^{11}\text{B}\{^1\text{H}\}$ NMR spectrum for the dimer is a sharp doublet at -19.74 ppm ($^1J_{11\text{B},31\text{P}}$ 60 Hz) in C_6D_6 , and remains a sharp doublet even at 110 °C in d_8 -toluene. The reactivity of $(\text{Me}_2\text{PCH}_2\text{BMe}_2)_2$ contrasts that of the aluminium analogue, $(\text{Me}_2\text{PCH}_2\text{AlMe}_2)_2$, which reacted with the aforementioned transition metal compounds at room temperature (*vide supra*).¹⁴ However, reactions of $(\text{Me}_2\text{PCH}_2\text{BMe}_2)_2$ with $\{[\text{M}(\mu\text{-Cl})(\text{cod})]_2\}$ (cod = 1,5-cyclooctadiene; M = Ir, Rh) and $[\text{PtCl}_2(\text{cod})]$ did proceed at elevated temperature.

In the case of $\{[\text{Ir}(\mu\text{-Cl})(\text{cod})]_2\}$, the 1:1 reaction with $(\text{Me}_2\text{PCH}_2\text{BMe}_2)_2$ at 65 °C afforded bright orange $[\text{Ir}(\text{cod})(\mu\text{-Cl})(\text{Me}_2\text{PCH}_2\text{BMe}_2)]_2$ (**1**; Scheme 3). Compound **1** was isolated in quantitative yield, and X-ray quality crystals (Figure 2) were obtained from CH_2Cl_2 /hexanes at -30 °C; crystals of **1** contain two independent but isostructural molecules within the unit cell. The geometry at iridium is square planar, with angles in the square plane ranging from 86.25° to 95.21°, and the borane is coordinated to the chloride ligand on iridium. The Ir–P distances are 2.3039(6) and 2.3033(6) Å, and the Ir–C distances range from 2.107(2) to 2.225(2) Å. The Ir–Cl distances are 2.3602(5) and 2.3647(6) Å, the B–Cl

distances are 2.272(3) Å and 2.240(3) Å, and the borane is appreciably pyramidalized, with the sum of the C–B–C angles equal to 349.2(6)° and 349.4(6)°.

The Ir–Cl bond in **1** is not significantly elongated relative to that in [IrCl(PMe₃)(cod)] (2.3538(5) Å)²⁰ or [IrCl(PEt₃)(cod)] (2.362(1) Å),²¹ in keeping with previous studies of Rh–Cl–BR₃ bridging interactions.²² Other crystallographically characterized Ir–Cl–BR₃ interactions are not available for comparison, but the Ir–Cl distance in **1** is similar to the Ir–Cl distance of 2.3610(5) Å in [Ir(cod)(μ-Cl)(κ¹:η⁵-ⁱPr₂PC₅H₄)Zr(η⁷-C₇H₇)], where the chloride ligand on iridium interacts with a pendent zirconium centre.²³ The B–Cl distance in **1** is approximately 0.2 Å longer than that in zwitterionic ClB(C₈H₁₄)(CH₂)₃NMe₂ⁿBu²⁴ or ClB(C₈H₁₄)(CH₂)₃PPh₃²⁵ (B(C₈H₁₄) = 9-borabicyclononyl), and the borane is less pyramidalized (B–Cl = 2.030(2)–2.065(3) Å and Σ(C–B–C) = 336.6–339.4° in the literature compounds).

The room temperature ¹¹B{¹H} NMR spectrum for compound **1** supports the presence of the Cl–BR₃ interaction in solution, with a single broad peak at 75.5 ppm in CD₂Cl₂,[†] which is shifted to low frequency relative to that for trialkylboranes such as BEt₃ (¹¹B NMR δ ~84 ppm).²⁶ However, it is notable that the ¹¹B NMR signal shifted to significantly lower frequency as the temperature was lowered, reaching a value of 65.9 ppm in CD₂Cl₂ at –80 °C (Figure 3). This is suggestive of a rapid equilibrium between structures in which the borane is either coordinated or un-coordinated to the chloride co-ligand (Figure 3), shifting in the direction of the entropically-disfavoured coordinated form at lower temperature. Given that compound **1** exists as the coordinated isomer in the solid state, a solid state ¹¹B NMR spectrum was obtained, affording a chemical shift of 40.5 ppm. Assigning values of 40.5 and 84.0 ppm to the coordinated and un-coordinated isomers of **1** afforded equilibrium constants of 4.1 and 1.4 for the reaction in Figure 3 at 25 and –80 °C in CD₂Cl₂, respectively.

Attempts to coordinate more than one equivalent of the Me₂PCH₂BMe₂ ligand to iridium by heating a solution of [{Ir(μ-Cl)(cod)}₂] and excess (Me₂PCH₂BMe₂)₂ at 65 °C were unsuccessful, and only **1** was observed as a product.

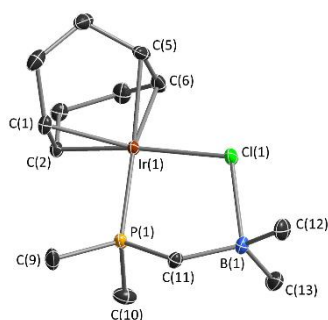


Figure 2. X-ray crystal structure of [Ir(cod)(μ-Cl)(Me₂PCH₂BMe₂)] (**1**). Only one of two independent molecules in the unit cell is shown. Ellipsoids are set to 50% probability, and hydrogen atoms have been omitted for clarity.

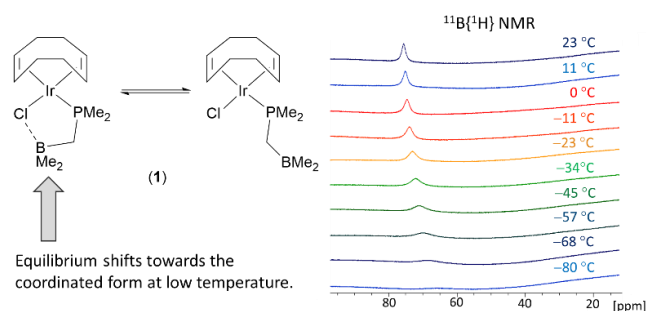


Figure 3. Equilibrium between coordinated and non-coordinated forms of compound **1**, and variable temperature ¹¹B{¹H} NMR spectra of **1**.

The reactivity of [{Rh(μ-Cl)(cod)}₂] with (Me₂PCH₂BMe₂)₂ at 65 °C differs from that of the iridium analogue, affording a mixture of [Rh(cod)(μ-Cl)(Me₂PCH₂BMe₂)] (**2**) and remaining [{RhCl(cod)}₂] and (Me₂PCH₂BMe₂)₂ after 48 hours, with no change after heating for 72 hours (Scheme 3). Additionally, attempts to crystallize the reaction product from this mixture yielded yellow 1:1 co-crystals of **2** and [{Rh(μ-Cl)(cod)}₂], and clear colourless crystals of the (Me₂PCH₂BMe₂)₂ dimer (Figure 4). The solid-state structure of **2** (Figure 4) is analogous to that of **1**, with a square planar geometry at rhodium and a Rh–Cl–BR₃ bridging interaction. The Rh–P distance is 2.2958(5) Å, and the Rh–C distances range from 2.107(2) to 2.248(2) Å. The Rh–Cl distance is 2.3811(5) Å, the B–Cl distance is 2.190(2) Å, and the sum of the C–B–C bond angles is 348.3(6)°. The shorter B–Cl distance and marginally increased pyramidalization at boron in **2** versus **1** are indicative of a slightly stronger B–Cl interaction in **2**, likely due to weaker M–Cl bonding in the rhodium complex. The ¹¹B NMR chemical shift of 65.2 ppm[†] for **2** in CD₂Cl₂ at room temperature decreased to 49.0 ppm at –91 °C. The room and low temperature ¹¹B NMR chemical shifts are significantly lower frequency than the those for **1**, consistent with a stronger B–Cl interaction in **2**.

The reduced favourability of Me₂PCH₂BMe₂ coordination to rhodium vs iridium (evident from the formation of an equilibrium mixture of **2** and the starting materials, and from calculated ΔG_{298K} values of –15 and +2 kJ mol^{–1}, respectively, for the reactions of 0.5 equiv. of (Me₂PCH₂BMe₂)₂ and [M(μ-Cl)(cod)]₂ to form **1** and **2**) presumably occurs due to weaker M–PR₃ coordination in **2**, despite the formation of a stronger Cl–BR₃ interaction. The Cl–BR₃ interaction in **2** can also be compared with the Cl–AlR₃ interaction in the previously reported aluminium analogue, [Rh(cod)(μ-Cl)(Me₂PCH₂AlMe₂)] (**3**); the Rh–Cl distance of 2.4176(3) Å in the alane complex is significantly longer than that in **2**, indicative of a stronger Cl–ER₃ (E = B or Al) interaction, consistent with the greater Lewis acidity of alanes versus boranes.^{27–29} However, it should be noted that the group 13 element is only marginally more pyramidalized in the alane complex (Σ(C–E–C) = 346.7° vs 348.3 in **2**).

The reactivity of (Me₂PCH₂BMe₂)₂ with [PtX₂(cod)] (X = Cl, Me) was also explored. The 1:1 reaction of (Me₂PCH₂BMe₂)₂ with [PtCl₂(cod)] at 65 °C afforded clear colourless crystals of [Pt(μ-Cl)₂(Me₂PCH₂BMe₂)₂] (**3**; Scheme 3 and Figure 5), with 2 independent but isostructural molecules of **3** in the unit cell. The geometry at platinum is square planar, and both chloride ligands are coordinated to a pendent borane. The Pt–P distances range from 2.216(5) to

2.241(5) Å, and the Pt–Cl distances from 2.363(5) to 2.411(5) Å. The B–Cl distances range from 2.14(2) to 2.19(2) Å, and the sum of the C–B–C angles at each boron centre are 345.6(6), 347.9(6), 347.5(6) and 352.5(6)°. A single ^{11}B NMR chemical shift was observed at 37.8 ppm in CD_2Cl_2 ,[†] which is indicative of stronger Cl–BR₃ interactions than in **1** and **2**. This can be rationalized by considering that each chloride ligand in **3** is *trans* to a phosphine, whereas the chloride ligand in **1** and **2** is *trans* to a lower *trans*-influence alkene ligand.³⁰ Compound **2** is to the best of our knowledge the first example of a monometallic transition metal complex featuring two M–Cl–BR₃ interactions. By contrast, $(\text{Me}_2\text{PCH}_2\text{BMe}_2)_2$ did not react with $[\text{PtMe}_2(\text{cod})]$, even after heating at 75 °C for 48 hours.

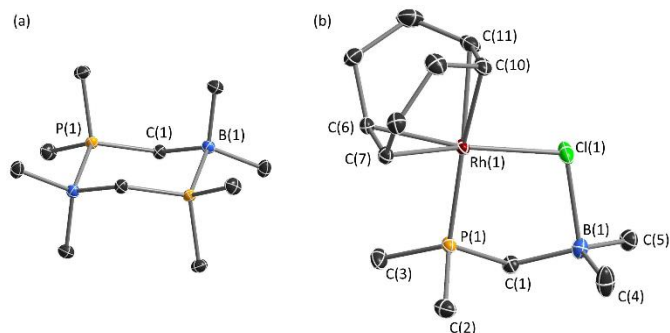


Figure 4. X-ray crystal structures of (a) $(\text{Me}_2\text{PCH}_2\text{BMe}_2)_2$, and (b) the boron-containing portion of $[\text{Rh}(\text{cod})(\mu\text{-Cl})(\text{Me}_2\text{PCH}_2\text{BMe}_2)] \cdot \{[\text{Rh}(\mu\text{-Cl})(\text{cod})]_2\}$ (**2**· $[\text{Rh}(\mu\text{-Cl})(\text{cod})]_2$). Ellipsoids are set to 50% probability, and hydrogen atoms have been omitted for clarity.

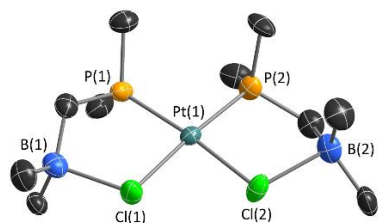


Figure 5. X-ray crystal structure of $[\text{Pt}(\mu\text{-Cl})_2(\text{Me}_2\text{PCH}_2\text{BMe}_2)_2]$ (**3**). Ellipsoids are set to 50% probability, and hydrogen atoms have been omitted for clarity.

The $\text{Me}_2\text{PCH}_2\text{BMe}_2$ ligand, unlike the aluminium analogue, shows no propensity for rearrangement by cleavage of the B–C bonds. However, the formation of an equilibrium mixture of **2** and the starting materials in the reaction of $(\text{Me}_2\text{PCH}_2\text{BMe}_2)_2$ with $[\{\text{Rh}(\mu\text{-Cl})(\text{cod})\}_2]$ highlights the extent to which $\text{Me}_2\text{PCH}_2\text{BMe}_2$ dimerization disfavors complex formation (by increasing the thermodynamic driving force for formation of the un-complexed ligand through dimerization). This is illustrated by DFT calculations (ADF/AMS, gas-phase, all-electron, PBE0, D3-BJ, TZ2P, scalar ZORA) which afforded very similar $\Delta G_{298\text{K}}$ values for (a) the reaction of monomeric $\text{Me}_2\text{PCH}_2\text{BMe}_2$ with 0.5 equiv. of $[\{\text{Rh}(\mu\text{-Cl})(\text{cod})\}_2]$ to afford **2** (-65 kJ mol^{-1}), and (b) $\text{Me}_2\text{PCH}_2\text{BMe}_2$ dimerization to afford 0.5 equiv. of the dimer (-67 kJ mol^{-1}). By contrast, calculated $\Delta G_{298\text{K}}$ values for the analogous reactions with $\text{Ph}_2\text{PCH}_2\text{BMe}_2$ are -61 and -50 kJ mol^{-1} , respectively, suggesting that phenyl substituents on phosphorus will yield a superior ligand, contrary to expectations if dimer formation is not considered.

The novel ligand precursor $(\text{Ph}_2\text{PCH}_2\text{BMe}_2)_2$ was prepared (Scheme 2) analogously to $(\text{Me}_2\text{PCH}_2\text{BMe}_2)_2$, via the addition of BrBMe_2 to $\text{LiCH}_2\text{PPh}_2$.³¹ Crystals were obtained from

hexanes/toluene (1:2) at $-30 \text{ }^\circ\text{C}$, and X-ray diffraction (Figure 6) revealed a B–P distance of 2.014(2) Å, which is longer than that for $(\text{Me}_2\text{PCH}_2\text{BMe}_2)_2$ (1.9783(6) Å), consistent with weaker P–B coordination (for comparison, the B–P distances in $(\text{Me}_2\text{PCH}_2\text{BCy}_2)_2$ ³² and $(\text{Ph}_2\text{PCH}_2\text{BPh}_2)_2$ ³³ are 1.998(2) and 2.00(1)/2.00(3) Å, respectively). The $^{11}\text{B}\{^1\text{H}\}$ NMR signal for $(\text{Ph}_2\text{PCH}_2\text{BMe}_2)_2$ is also a broad singlet (-15.3 ppm in C_6D_6), compared with a sharp doublet for $(\text{Me}_2\text{PCH}_2\text{BMe}_2)_2$ (-19.74 ppm in C_6D_6 ; $^1J_{\text{P-B}} 60 \text{ Hz}$), perhaps indicative of some degree of phosphine-borane dissociation for $(\text{Ph}_2\text{PCH}_2\text{BMe}_2)_2$ in solution at room temperature (*vide infra*). That said, boron is marginally more pyramidalized in the X-ray structure of the phenyl-substituted compound ($\Sigma(\text{C-B-C}) = 333.5(3)$, versus $335.2(1)^\circ$ in the methyl analogue), possibly due to coordination to a more sterically encumbered phosphine.

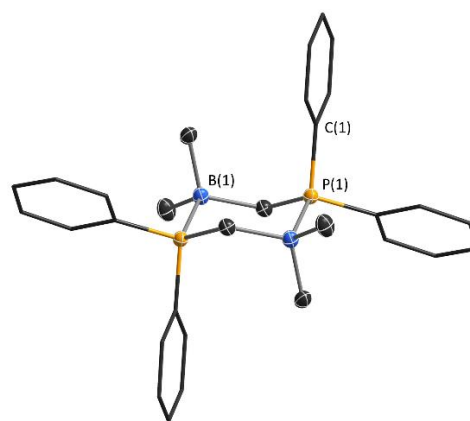
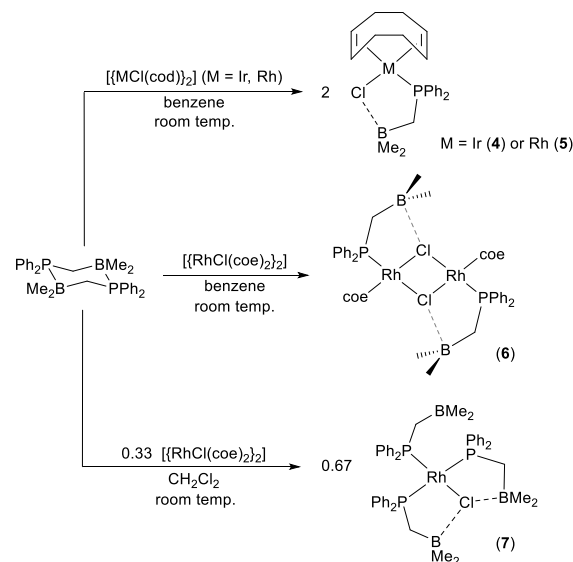


Figure 6. X-ray crystal structure of $(\text{Ph}_2\text{PCH}_2\text{BMe}_2)_2$. Ellipsoids are set to 50% probability, hydrogen atoms have been omitted, and phenyl rings are shown in wireframe for clarity.



Scheme 4. Reactions of $(\text{Ph}_2\text{PCH}_2\text{BMe}_2)_2$ to form complexes **4-7**.

Addition of 1 equivalent of $(\text{Ph}_2\text{PCH}_2\text{BMe}_2)_2$ to $[\{\text{Ir}(\mu\text{-Cl})(\text{cod})\}_2]$ in CH_2Cl_2 yielded orange-red $[\text{Ir}(\text{cod})(\mu\text{-Cl})(\text{Ph}_2\text{PCH}_2\text{BMe}_2)]_2$ (**4**; Scheme 4). This reaction was complete after one hour at room temperature, contrasting the analogous reaction with $(\text{Me}_2\text{PCH}_2\text{BMe}_2)_2$ which required heating at $65 \text{ }^\circ\text{C}$ for 24 hours to reach completion. This reactivity suggests that the $(\text{Ph}_2\text{PCH}_2\text{BMe}_2)_2$ dimer dissociates (one

or both P–B bonds) in solution at room temperature, consistent with the broad $^{11}\text{B}\{^1\text{H}\}$ NMR signal for $(\text{Ph}_2\text{PCH}_2\text{BMe}_2)_2$ (compared with a sharp doublet for $(\text{Me}_2\text{PCH}_2\text{BMe}_2)_2$), and the less negative ΔG calculated for dimerization of $\text{Ph}_2\text{PCH}_2\text{BMe}_2$ versus $\text{Me}_2\text{PCH}_2\text{BMe}_2$ (*vide supra*).

X-ray quality crystals of $4 \cdot 0.5 \text{CH}_2\text{Cl}_2$ (Figure 7) were obtained from $\text{CH}_2\text{Cl}_2/\text{hexanes}$ (1:10) at -30°C . The unit cell contains two independent and isostructural molecules of **4**, with a square planar geometry at iridium. The Ir–P distances are 2.298(1) and 2.301(1) Å, and the Ir–C distances range from 2.115(5) to 2.221(5) Å. The Ir–Cl distances are 2.356(1) and 2.369(1) Å, the B–Cl distances are 2.283(6) and 2.250(6) Å, and the sums of the C–B–C bond angles are $351(2)$ and $350(1)^\circ$; these bond metrics are very similar to those in $[\text{Ir}(\text{cod})(\mu\text{-Cl})(\text{Me}_2\text{PCH}_2\text{BMe}_2)]$ (**1**), as expected given that the substituents on boron are unchanged. Compound **4** gave rise to a room temperature ^{11}B NMR signal at 51.3 ppm in CD_2Cl_2 ,[†] which decreased to 45.1 ppm at -57°C . The room temperature ^{11}B NMR chemical shift for **4** is significantly lower frequency than that for **1** (75.5 ppm in CD_2Cl_2), which is surprising, given that a lower ^{11}B NMR chemical shift is typically taken as evidence of a stronger Lewis base–borane interaction. However, this may be explained by considering that (a) an equilibrium exists between coordinated and non-coordinated forms of **1** (see Figure 3) and **4**, and (b) this equilibrium lies significantly further towards the coordinated form for **4** due to a Thorpe–Ingold type effect³⁴ that arises from the steric influence of the substituents on phosphorus (which raises the energy of the acyclic un-coordinated form, pushing the equilibrium towards the coordinated form, despite very similar B–Cl interaction strengths in both compounds (**1** and **4**)). For both **1** and **4**, this equilibrium shifts towards the coordinated form at low temperature. However, it is notable that even at -80°C , the ^{11}B NMR chemical shift for **1** is at higher frequency than that of **4** at room temperature.

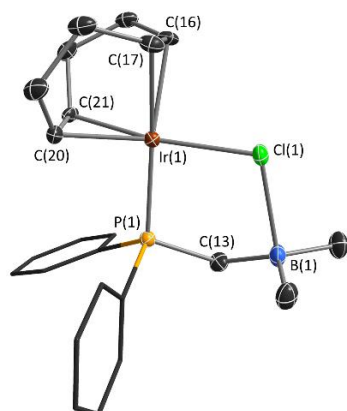


Figure 7. X-ray crystal structure of $[\text{Ir}(\text{cod})(\mu\text{-Cl})(\text{Ph}_2\text{PCH}_2\text{BMe}_2)] \cdot 0.5\text{CH}_2\text{Cl}_2$ (**4**· $0.5\text{CH}_2\text{Cl}_2$). Ellipsoids are set to 50% probability, hydrogen atoms and lattice solvent have been omitted, and phenyl rings are shown in wireframe for clarity.

The 1:1 reaction of $(\text{Ph}_2\text{PCH}_2\text{BMe}_2)_2$ with $[\{\text{Rh}(\mu\text{-Cl})(\text{cod})\}_2]$ was also complete after 1 hour at room temperature, affording $[\text{Rh}(\text{cod})(\mu\text{-Cl})(\text{Ph}_2\text{PCH}_2\text{BMe}_2)]$ (**5**; Scheme 4). This reactivity contrasts that of $(\text{Me}_2\text{PCH}_2\text{BMe}_2)_2$ with $[\{\text{Rh}(\mu\text{-Cl})(\text{cod})\}_2]$ which only proceeded slowly at 65°C , and afforded an equilibrium mixture of **2** and the starting materials (*vide supra*). X-ray quality crystals of $5 \cdot \text{CH}_2\text{Cl}_2$ were obtained from $\text{CH}_2\text{Cl}_2/\text{hexanes}$ at -30°C , and the structure of **5**

(Figure S64) was found to be analogous to the iridium counterpart (**4**; Figure 7), including the presence of two independent molecules in the unit cell. Rhodium in **5** is square planar, with Rh–C distances ranging from 2.120(3) to 2.249(3) Å, Rh–P distances of 2.2958(8) and 2.2910(8) Å, and Rh–Cl distances of 2.3769(8) and 2.3663(8) Å. The B–Cl distances of 2.186(3) and 2.210(4) Å in **5** are comparable with those in the $\text{Me}_2\text{PCH}_2\text{BMe}_2$ analogue (**2**), as are the sums of the C–B–C angles, which are $348.9(9)$ and $347.2(9)^\circ$. The ^{11}B NMR chemical shift is 39.3 ppm in CD_2Cl_2 at room temperature,[†] and 35.9 ppm at -57°C . These chemical shifts are lower frequency than those for **2** (65.2 ppm at room temperature and 49.0 ppm at -91°C in CD_2Cl_2).

Reactions of $[\{\text{M}(\mu\text{-Cl})(\text{cod})\}_2]$ (M = Ir or Rh) with excess $(\text{Ph}_2\text{PCH}_2\text{BMe}_2)_2$ only generated **4** and **5**, even after heating for 12 hours at $65\text{--}70^\circ\text{C}$. However, $[\{\text{Rh}(\mu\text{-Cl})(\text{coe})_2\}_2]$ (coe = cyclooctene) reacted with either 1 or 3 equivalents of $(\text{Ph}_2\text{PCH}_2\text{BMe}_2)_2$ in CH_2Cl_2 to cleanly generate $[\{\text{Rh}(\text{coe})(\mu\text{-Cl})(\text{Ph}_2\text{PCH}_2\text{BMe}_2)_2\}_2]$ (**6**) and $[\text{RhCl}(\text{Ph}_2\text{PCH}_2\text{BMe}_2)_3]$ (**7**), respectively (Scheme 4),[†] and X-ray quality crystals of $6 \cdot 2 \text{CH}_2\text{Cl}_2$ and **7** (Figures 8 and 9) were obtained at -30°C from CH_2Cl_2 (for **6**) or toluene/hexanes (for **7**).

Compound **6** (Figure 8) is a dimer with chloride ligands bridging between square planar rhodium centres. Each metal centre is additionally bound to one cyclooctene ligand and the phosphine donor of $\text{Ph}_2\text{PCH}_2\text{BMe}_2$, with a Rh–P distance of 2.192(1) Å, Rh–C distances of 2.115(3) and 2.118(3) Å, and Rh–Cl(1) and Rh–Cl(1') distances of 2.387(1) and 2.491(1) Å. Each borane in the solid state structure of **6** is slightly pyramidalized and interacts weakly with a bridging chloride ligand ($\Sigma(\text{C–B–C}) = 358(1)$; B–Cl = 2.687(5) Å). Additionally, the room temperature $^{11}\text{B}\{^1\text{H}\}$ NMR chemical shift is 77.6 ppm in CD_2Cl_2 , which is slightly lower than that expected for a free trialkylborane, supporting the presence of a weak B–Cl interaction in solution. To the best of our knowledge, **6** is the first example of a pendent borane interacting with a bridging halide ligand.

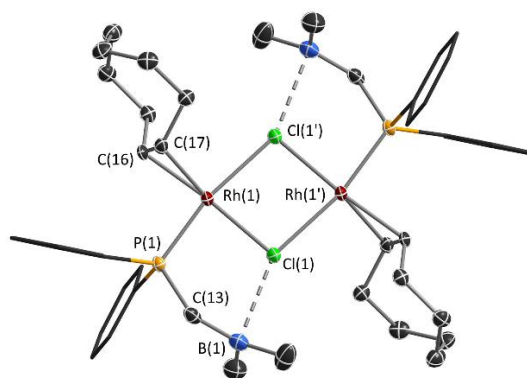


Figure 8. X-ray crystal structure of $[\{\text{Rh}(\text{coe})(\mu\text{-Cl})(\text{Ph}_2\text{PCH}_2\text{BMe}_2)_2\}_2] \cdot 2\text{CH}_2\text{Cl}_2$ (**6**· $2\text{CH}_2\text{Cl}_2$). Ellipsoids are set to 50% probability, hydrogen atoms and lattice solvent have been omitted, and phenyl rings are shown in wireframe for clarity.

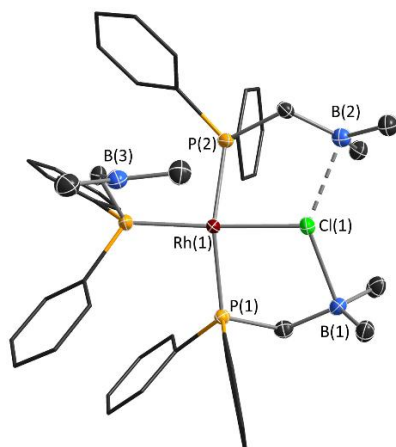


Figure 9. X-ray crystal structure of $[\text{RhCl}(\text{Ph}_2\text{PCH}_2\text{BMe}_2)_3]$ (**7**). Ellipsoids are set to 50% probability, hydrogen atoms have been omitted, and phenyl rings are shown in wireframe for clarity.

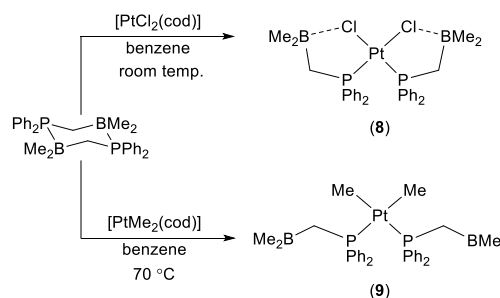
Compound **7** (Figure 9) is a borane-appended analogue of Wilkinson's catalyst, $[\text{RhCl}(\text{PPh}_3)_3]$. The unit cell of **7** contains two independent but isostructural molecules. The geometry at rhodium is distorted square planar, where (a) the two phosphines that are *trans* to one another are bent towards the chloride ligand, and (b) the geometry distorts slightly in the direction of a tetrahedron. This results in *trans* P–Rh–P angles of 158.69(3) and 159.89(4) $^\circ$ and *trans* P–Rh–Cl angles of 166.88(4) and 165.40(4) $^\circ$; $[\text{RhCl}(\text{PPh}_3)_3]$ is similarly distorted, resulting in *trans* P–Rh–P and *trans* P–Rh–Cl angles of 159.1(2) and 166.7(2) $^\circ$ (orange polymorph), or 152.8(1), 156.2(2) (red polymorph), respectively.³⁵ The Rh–P distances for the phosphines that are *trans* to one another in **7** range from 2.303(1) to 2.332(1) Å, whereas the Rh–P distance for the phosphine *trans* to chloride is 2.209(1)–2.216(1) Å. The Rh–Cl distances in **7** are 2.389(1) and 2.398(1) Å, and the chloride ligand is tightly coordinated to one borane (B–Cl = 2.298(4), 2.265(4) Å; $\Sigma(\text{C–B–C}) = 351(1), 349(1)^\circ$), and weakly coordinated to a second borane (B–Cl = 2.488(4), 2.504(5) Å; $\Sigma(\text{C–B–C}) = 355(1), 354(1)^\circ$). The third borane (in the ambiphilic ligand *trans* to chloride) is non-coordinated with a trigonal planar geometry ($\Sigma(\text{C–B–C}) = 360(1), 359(1)^\circ$).⁵

To the best of our knowledge, **7** is the first example of a complex in which two boranes interact with a single halide co-ligand. This is likely facilitated by the low steric hindrance of the boranes, and the formation of a favourable 5-membered ring. The electron rich metal centre and *trans*-influence of the phosphine donor presumably also contribute. For comparison, bulkier $\text{R}_2\text{PCH}_2\text{CH}_2\text{BC}_8\text{H}_{14}$ (R = Ph⁵ or 2-furyl);³⁶ BC_8H_{14} = 9-borabicyclononyl) ligands formed *trans*- $[\text{RhCl}(\text{CO})(\text{R}_2\text{PCH}_2\text{CH}_2\text{BC}_8\text{H}_{14})_2]$ complexes in which either one borane (R = Ph; Cl–B = 2.353(3) Å) or neither borane (R = 2-furyl) interacts with the chloride co-ligand in the solid state. By contrast, the less sterically-hindered but more rigid $\text{Me}_2\text{PCMe}=\text{CMeBMe}_2$ ligand afforded *trans*- $[\text{RhCl}(\text{CO})(\text{Me}_2\text{PCMe}=\text{CMeBMe}_2)_2]$ featuring two Rh–BR₃ interactions (Rh–B = 2.94(3) and 2.97(4) Å).³⁷ Formation of a rhodium–borane interaction in **7** is presumably disfavoured by the short linker between the phosphine and the borane of

$\text{Ph}_2\text{PCH}_2\text{BMe}_2$, which would result in a strained 4-membered Rh–P–C–B ring.

The ^1H NMR spectra for **7** at 25 $^\circ\text{C}$ and -80 $^\circ\text{C}$ show two sets of $\text{Ph}_2\text{PCH}_2\text{BMe}_2$ signals in a 2:1 ratio, in each case with just one P–Ph (*o*, *m* and *p*), B–Me and CH_2 environment, indicative of apparent C_{2v} symmetry on the NMR timescale. Additionally, the room temperature $^{31}\text{P}\{^1\text{H}\}$ NMR spectrum of **7** in CD_2Cl_2 consists of a doublet of triplets at 41.17 ppm ($^1J_{\text{Rh-P}} = 198$ Hz, $^2J_{\text{P-P}} = 39$ Hz) and a doublet of doublets at 35.37 ppm ($^1J_{\text{Rh-P}} = 137$ Hz, $^2J_{\text{P-P}} = 39$ Hz), and two signals with the same coupling pattern were observed at -80 $^\circ\text{C}$. The $^{11}\text{B}\{^1\text{H}\}$ NMR spectrum of **7** at room temperature in CD_2Cl_2 contains two broad peaks at 84.5 and 50.7 ppm, the latter of which corresponds to the two boranes interacting with the chloride ligand. No splitting of this peak was observed down to -45 $^\circ\text{C}$, and below this temperature this signal was too broad to observe.

Finally, coordination of $\text{Ph}_2\text{PCH}_2\text{BMe}_2$ to platinum was explored. Addition of one equivalent of $(\text{Ph}_2\text{PCH}_2\text{BMe}_2)_2$ to $[\text{PtCl}_2(\text{cod})]$ in dichloromethane at room temperature formed $[\text{Pt}(\mu\text{-Cl})_2(\text{Ph}_2\text{PCH}_2\text{BMe}_2)_2]$ (**8**) over the course of an hour (Scheme 5). Characterization of this complex by X-ray diffraction (Figure 10) revealed a square planar structure analogous to that of $[\text{Pt}(\mu\text{-Cl})_2(\text{Me}_2\text{PCH}_2\text{BMe}_2)_2]$ (**3**), with the phosphine-borane ligands *cis* to one another, and each borane interacting with one chloride ligand (B–Cl = 2.186(4), 2.181(4) Å; $\Sigma(\text{C–B–C}) = 348.6(9), 348.1(9)^\circ$). These distances and angles are comparable with those in **3**. The Pt–P distances are 2.2455(8) and 2.2531(8) Å, and the Pt–Cl distances are 2.3724(8) and 2.3660(8) Å. The room temperature ^{11}B NMR chemical shift is 36.3 ppm in CD_2Cl_2 ,[†] which is similar to that for **3** (37.8 ppm), and the ^{11}B NMR chemical shift for **8** shifted only slightly to 33.5 ppm upon lowering the temperature to -34 $^\circ\text{C}$ (below this temperature the boron signal was not observed due to poor solubility).



Scheme 5. Reactions of $(\text{Ph}_2\text{PCH}_2\text{BMe}_2)_2$ to form complexes **8** and **9**.

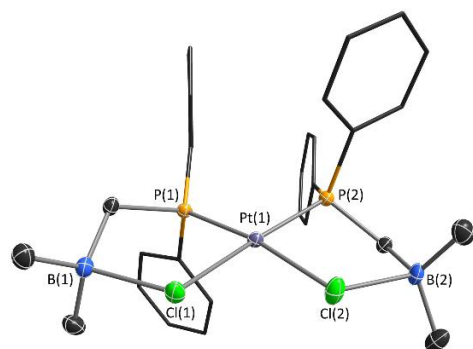


Figure 10. X-ray crystal structure of $[\text{Pt}(\mu\text{-Cl})_2(\text{Ph}_2\text{PCH}_2\text{BMe}_2)_2]$ (**8**). Ellipsoids are set to 50% probability, hydrogen atoms have been omitted, and phenyl rings are shown in wireframe for clarity.

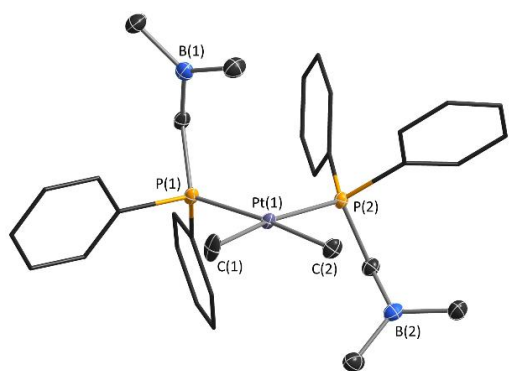


Figure 11. X-ray crystal structure of $[\text{PtMe}_2(\text{Ph}_2\text{PCH}_2\text{BMe}_2)_2]$ (**9**). Ellipsoids are set to 50% probability, hydrogen atoms have been omitted, and phenyl rings are shown in wireframe for clarity.

When $(\text{Ph}_2\text{PCH}_2\text{BMe}_2)_2$ was heated with one equivalent of $[\text{PtMe}_2(\text{cod})]$ at 70 °C, five signals with $^{195}\text{Pt}\text{-}^{31}\text{P}$ coupling were observed by $^{31}\text{P}\{^1\text{H}\}$ NMR spectroscopy; one major signal ($\sim 75\%$) at 17.56 ppm, and four smaller signals at 23.04, -33.38, -50.06 and -51.83 ppm. The major product was isolated (Scheme 5) by sonication in hexanes to give a pale yellow powder, followed by selective recrystallization from $\text{CH}_2\text{Cl}_2/\text{hexanes}$ at -30 °C. This compound was identified as $cis\text{-}[\text{PtMe}_2(\text{Ph}_2\text{PCH}_2\text{BMe}_2)_2]$ by single crystal X-ray diffraction (Figure 11), with Pt–P distances of 2.2869(8) and 2.3040(9) Å, and Pt–C distances of 2.088(3) and 2.096(3) Å. Unlike compound **8**, both boranes in **9** are planar ($\Sigma(\text{C}–\text{B}–\text{C}) = 359.7(8), 360(1)^\circ$), and do not interact (via boron) with platinum or the methyl co-ligands; the shortest $\text{Pt}\cdots\text{B}$ and $\text{C}_{\text{PtMe}}\cdots\text{B}$ distances are 3.74 and 3.19 Å, respectively.⁵ Compound **9** gave rise to ^1H NMR signals for the PtMe and BMe groups at 1.06 ($^2J_{\text{H,Pt}} = 68$ Hz) and 0.92 ppm, respectively, and an ^{11}B NMR signal at 84 ppm, consistent with free pendent boranes. The room temperature PtMe ^1H NMR signals for **9** are sharp, and 2D EXSY NMR did not reveal any evidence for methyl exchange between platinum and boron.

Summary and Conclusions

A more straightforward synthesis for $(\text{Me}_2\text{PCH}_2\text{BMe}_2)_2$ is reported, and this method was extended to the synthesis of previously unreported $(\text{Ph}_2\text{PCH}_2\text{BMe}_2)_2$. The transition metal

chemistry of $\text{R}_2\text{PCH}_2\text{BMe}_2$ ligands has not previously been investigated, and notable features of the ligands are: (a) the 1-atom linker between phosphorus and boron, which may be expected to favour interactions with substrates and co-ligands versus metal–borane coordination (to avoid the formation of a 4-membered metallacycle), and (b) the low steric requirement of the substituents on boron; most other ambiphilic ligands with hydrocarbyl substituents on boron employ aryl groups (e.g. $\text{BR}_2 = \text{BPh}_2$ or BMe_2) or bulky alkyl groups (e.g. $\text{BR}_2 = \text{BCy}_2$ or 9-borabicyclononyl).

The ligand precursor $(\text{Me}_2\text{PCH}_2\text{BMe}_2)_2$ did not react with $[\{\text{M}(\mu\text{-Cl})(\text{cod})\}_2]$ ($\text{cod} = 1,5\text{-cyclooctadiene}$; $\text{M} = \text{Rh}$ and Ir) or $[\text{PtCl}_2(\text{cod})]$ ($\text{X} = \text{Me}, \text{Cl}$) at room temperature. However, at 65 °C, these reactions slowly proceeded to afford (a) $[\text{Ir}(\text{cod})(\mu\text{-Cl})(\text{Me}_2\text{PCH}_2\text{BMe}_2)]$ (**1**), (b) an equilibrium mixture of $(\text{Me}_2\text{PCH}_2\text{BMe}_2)_2$, $[\{\text{Rh}(\mu\text{-Cl})(\text{cod})\}_2]$ and $[\text{Rh}(\text{cod})(\mu\text{-Cl})(\text{Me}_2\text{PCH}_2\text{BMe}_2)]$ (**2**), and (c) $cis\text{-}[\text{Pt}(\mu\text{-Cl})_2(\text{Me}_2\text{PCH}_2\text{BMe}_2)_2]$ (**3**), respectively. By contrast, $(\text{Ph}_2\text{PCH}_2\text{BMe}_2)_2$ reacted with $[\{\text{M}(\mu\text{-Cl})(\text{cod})\}_2]$ ($\text{cod} = 1,5\text{-cyclooctadiene}$; $\text{M} = \text{Rh}$ and Ir) at room temperature to rapidly generate $[\text{M}(\text{cod})(\mu\text{-Cl})(\text{Ph}_2\text{PCH}_2\text{BMe}_2)]$ ($\text{M} = \text{Ir}$ (**4**) and Rh (**5**)), indicative of room temperature $(\text{Ph}_2\text{PCH}_2\text{BMe}_2)_2$ dissociation. Reactions of $(\text{Ph}_2\text{PCH}_2\text{BMe}_2)_2$ with $[\{\text{Rh}(\mu\text{-Cl})(\text{coe})\}_2]$ ($\text{coe} = \text{cyclooctene}$) using a 1:1 or 3:1 stoichiometry afforded $[\{\text{Rh}(\text{coe})(\mu\text{-Cl})(\text{Ph}_2\text{PCH}_2\text{BMe}_2)_2\}_2]$ (**6**) and $[\text{RhCl}(\text{Ph}_2\text{PCH}_2\text{BMe}_2)_3]$ (**7**), where the latter is a borane-appended analogue of Wilkinson's catalyst, and reactions of $(\text{Ph}_2\text{PCH}_2\text{BMe}_2)_2$ with $[\text{PtX}_2(\text{cod})]$ ($\text{X} = \text{Cl}$ or Me) yielded $cis\text{-}[\text{Pt}(\mu\text{-Cl})_2(\text{Ph}_2\text{PCH}_2\text{BMe}_2)_2]$ (**8**) and $cis\text{-}[\text{PtMe}_2(\text{Ph}_2\text{PCH}_2\text{BMe}_2)_2]$ (**9**).

To the best of our knowledge, compounds **3** and **8** are the first monometallic transition metal complexes featuring two $\text{M}–\text{Cl}–\text{BR}_3$ interactions, and **6** provides the first example of a pendent borane interacting (albeit weakly) with a bridging halide ligand. In addition, **7** appears to be the first ambiphilic ligand complex in which two group 13 Lewis acids interact with a single halide co-ligand. Both boranes in **9**, and one of the three boranes in **7**, are non-coordinated.

The $\text{R}_2\text{PCH}_2\text{BMe}_2$ ($\text{R} = \text{Me}$ or Ph) ligands, unlike $\text{Me}_2\text{PCH}_2\text{AlMe}_2$,¹⁴ show no propensity for rearrangement by cleavage of the $\text{B}–\text{C}$ linkages. However, the formation of an equilibrium mixture of **2** and the starting materials in the reaction of $(\text{Me}_2\text{PCH}_2\text{BMe}_2)_2$ with $[\{\text{Rh}(\mu\text{-Cl})(\text{cod})\}_2]$ highlights the extent to which $\text{Me}_2\text{PCH}_2\text{BMe}_2$ dimerization disfavours complex formation. In comparison, phenyl-substituted $\text{Ph}_2\text{PCH}_2\text{BMe}_2$ is a superior ligand, as evidenced by complete conversion of $(\text{Ph}_2\text{PCH}_2\text{BMe}_2)_2$ and $[\{\text{Rh}(\mu\text{-Cl})(\text{cod})\}_2]$ to **5**. This occurs because $\text{Ph}_2\text{PCH}_2\text{BMe}_2$ dimerization is disfavoured relative to complex formation; calculated ΔG values (at 298 K) for $\text{R}_2\text{PCH}_2\text{BMe}_2$ dimerization are -67 and -50 kJ mol^{-1} for the methyl versus the phenyl-substituted ligands, and the ΔG values for reaction of monomeric $\text{R}_2\text{PCH}_2\text{BMe}_2$ ($\text{R} = \text{Me}$ or Ph) with 0.5 equiv. of $[\{\text{Rh}(\mu\text{-Cl})(\text{cod})\}_2]$ to afford **2** or **5** are -65 and -61 kJ mol^{-1} , respectively.

Variable temperature ^{11}B NMR data for compounds **1–2** and **4–5** suggest that (a) a rapid equilibrium exists in solution between structures (e.g. **1** in Figure 3) in which the borane is either coordinated or non-coordinated to the chloride co-

ligand, and (b) this equilibrium lies much further towards the coordinated species for **4** and **5** compared to **1** and **2**, despite similar Cl–BR₃ interaction strengths (indicated by very similar B–Cl distances and boron pyramidalization in the solid state; as expected considering that the substituents on boron are identical). This can be explained by a Thorpe-Ingold type effect,³⁴ where the steric influence of the phenyl substituents in the Ph₂PCH₂BMe₂ complexes (**4-5**) raises the energy of the acyclic un-coordinated form. Consequently, with the Ph₂PCH₂BMe₂ ligand, the equilibrium lies further towards the coordinated form, despite very similar Cl–BR₃ interaction strengths in complexes of Ph₂PCH₂BMe₂ and Me₂PCH₂BMe₂ (**1** vs **4** and **2** vs **5**).

Investigations into the reactivity of R₂PCH₂BMe₂ complexes, with small molecules are ongoing.

Experimental Section

General Details: All chemistry was carried out using standard techniques³⁸ under an argon atmosphere in an MBraun Unilab glovebox equipped with a –30 °C freezer, or on a double manifold vacuum line. The vacuum was measured periodically using a Kurt J. Lesker 275i convection enhanced Pirani gauge. Residual oxygen and moisture was removed from the argon stream by passage through an Oxisorb-W scrubber from Matheson Gas Products.

Benzene, pentane, hexanes, toluene, tetrahydrofuran (THF), and diethyl ether (Et₂O) were purchased from Sigma Aldrich. These solvents were initially dried and distilled at atmospheric pressure from sodium (toluene) or sodium/benzophenone (the other five solvents). All solvents were stored over an appropriate drying agent (benzene, toluene, OEt₂, THF = Na/Ph₂CO; hexanes, pentane = Na/Ph₂CO/tetraglyme) and introduced to reactions or solvent storage flasks via vacuum transfer with condensation at –78 °C. Anhydrous dichloromethane was purchased from Sigma Aldrich, dried over molecular sieves (4 Å), and distilled. Deuterated solvents were purchased from Cambridge Isotope Laboratories: C₆D₆ (99.5%) was dried over sodium/benzophenone, distilled prior to use, and stored under argon. CD₂Cl₂ (99.8%) was dried over molecular sieves (4 Å), distilled prior to use, and stored under argon.

PMe₃ and BrBMe₂ were purchased from Sigma-Aldrich. A solution of ^tBuLi (1.7 M in pentane) was purchased from Sigma-Aldrich and then evaporated to dryness to afford solid ^tBuLi as a white solid. [{Rh(μ-Cl)(cod)}₂] was purchased from Pressure Chemicals and [{Ir(μ-Cl)(cod)}₂] was purchased from Strem Chemicals. [PtCl₂(cod)],³⁹ [PtR₂(cod)] (R = CH₃ or CD₃)⁴⁰, MePPh₂,⁴¹ LiCH₂PMe₂,⁴² and LiCH₂PPh₂,³¹ were synthesized according to literature procedures.

NMR spectroscopy (¹H, ¹³C{¹H}, ³¹P{¹H}, ¹¹B{¹H}, COSY, HSQC, HMBC, NOESY) was performed on Bruker AV-500 and AV-600 spectrometers. Spectra were obtained at 298 K unless otherwise indicated. All ¹H NMR spectra were referenced relative to SiMe₄ through a resonance of the proteo impurity of the solvent used: C₆D₆ (δ 7.16 ppm), CD₂Cl₂ (δ 5.32 ppm) and d⁸-toluene (δ 2.08 ppm, 6.97 ppm, 7.01 ppm, and 7.09 ppm). All

¹³C NMR spectra were referenced relative to SiMe₄ through a ¹³C resonance of the solvent: C₆D₆ (δ 128.06 ppm), CD₂Cl₂ (δ 54.00 ppm) and d⁸-toluene (δ 20.43, 125.13, 127.96, 128.87, and 137.48 ppm). The ³¹P{¹H} and ¹¹B{¹H} NMR spectra were referenced using an external standard of 85% H₃PO₄ in D₂O (0.0 ppm) or neat BF₃(OEt₂) (0.0 ppm), or through indirect referencing.⁴³ Relative concentrations of species were determined by integration of ¹H NMR spectra, unless otherwise indicated.

The ¹¹B solid state NMR spectrum was acquired on a Bruker Avance III spectrometer operating at a Larmor frequency of 272.76 MHz (20 T, 850 MHz nominal ¹H frequency). The powder sample was packed into a 1.9 mm rotor and spun to 25 kHz for magic angle spinning experiments. A 90–180 spin echo sequence using an RF field strength of 70 kHz was used, and 512 scans were acquired with a relaxation time of 2.5 s. NaBH₄ was used as an external reference (δ –42 ppm, relative to δ 0 for BF₃·Et₂O). The resulting spectrum was deconvoluted using a one-site infinite MAS speed quadrupolar model using the dmfit software.⁴⁴

Single-crystal X-ray crystallographic analyses were performed at 100 K (unless otherwise stated) on crystals in Paratone oil. Crystals were mounted on a SMART APEX II diffractometer with a 3 kW sealed-tube Mo generator and APEX II CCD detector or a STOE IPDS II with a 3 kW sealed-tube Mo generator in the McMaster Analytical X-Ray (MAX) Diffraction Facility. Raw data was processed using SAINT, SADABS, and XPREP (as part of the Bruker APEX4 software package), and solved by intrinsic (SHELXT) methods. Structures were completed by difference Fourier synthesis and refined with full-matrix least-squares procedures based on *F*². In all cases, non-hydrogen atoms were refined anisotropically. Hydrogen atoms were generated in ideal positions and then updated with each cycle of refinement, which was performed using SHELXL in Olex2.

Combustion elemental analyses were performed by the University of Calgary.

(Me₂PCH₂BMe₂)₂

LiCH₂PMe₂ (1.65 g; 21.6 mmol) was suspended in 15 mL of Et₂O and cooled to –78 °C. 16.0 mL of a 1.45 M solution of BrBMe₂ in toluene was added dropwise. The cold bath was then removed, and the reaction was stirred for 12 hours at room temperature. After removal of volatiles *in vacuo*, the resulting crude product was sublimed at 90 °C (5–10 mTorr) to give 1.26 g (50.4% yield) of (Me₂PCH₂BMe₂)₂ as a white powder. C₁₀H₂₈B₂P₂ (231.90 g mol⁻¹) calcd. C 51.79 %, H 12.17%; found 51.49 %, H 12.05 %. ¹H NMR (600 MHz, 298 K, C₆D₆) δ: 0.72 (d, 6H, ²J_{H-P} = 9.8 Hz, (CH₃)₂P); 0.48 (broad s, 2H, PCH₂B); 0.02 (broad d, 6H, ³J_{P-H} = 16.8 Hz, B(CH₃)₂). ¹³C{¹H} NMR (150.9 MHz, 298K, C₆D₆, δ): 17.48 (m, PCH₂B); 9.37 (m, BMe₂); 9.11 (d, ¹J_{P-C} = 30 Hz, PMe₂). ³¹P{¹H} NMR (202.4 MHz, 298K, C₆D₆) δ: -5.37 (broad quartet, ¹J_{B-P} = 42 Hz). ¹¹B{¹H} NMR (192.5 MHz, 298K, C₆D₆) δ: -19.74 (d, ¹J_{P-B} = 59 Hz).

(Ph₂PCH₂BMe₂)₂

Solid $\text{LiCH}_2\text{PPh}_2$ (2.515 g, 12.2 mmol) was suspended in 20 mL of Et_2O in a round bottom flask. A solution of BrBMe_2 in toluene (11.3 mL, 1.18 M) was then added dropwise to the flask at -78°C . The cloudy white solution was allowed to come to room temperature slowly and was then stirred at room temperature for 12 hours. Solvent was removed *in vacuo*, and clear colorless impurities were distilled off at 110°C (at 5–10 mTorr). Subsequent sublimation at 165°C (at 5–10 mTorr) afforded $(\text{Ph}_2\text{PCH}_2\text{BMe}_2)_2$ as a white powder (0.9733 g, 32.6% yield). The product could also be recrystallized from a 1:2 hexanes/toluene mixture at -30°C , and X-ray quality crystals were obtained via this method. **$\text{C}_{30}\text{H}_{36}\text{B}_2\text{P}_2$ (480.18 g mol $^{-1}$):** calcd. C 75.04 %, H 7.56 %; found C 74.51 %, H 7.24 %. **$^1\text{H NMR}$ (600 MHz, 298 K, C_6D_6) δ :** 7.63 (m, 4H, *PPh*₂); 7.01 (m, 6H, *PPh*₂); 1.91 (dd, $^2J_{\text{P-H}} = 18.6$ Hz, $^3J_{\text{P-H}} = 13.2$ Hz, 2H, *PCH*₂B); 0.11 (d, $^3J_{\text{P-H}} = 16.6$ Hz, 6H, *BMe*). **$^{13}\text{C}\{^1\text{H}\}$ NMR (150.9 MHz, 298 K, C_6D_6) δ :** 133.80 (d, $^1J_{\text{P-C}} = 44.8$ Hz, *P-C_{ipso}*); 133.20 (d, $^2J_{\text{P-C}} = 8.0$ Hz, *P-C_{meta}*), 130.10 (d, $^4J_{\text{P-C}} = 1.6$ Hz, *P-C_{para}*), 128.41 (d, $^3J_{\text{P-C}} = 9.0$ Hz, *P-C_{ortho}*), 16.0 (bs, *PCH*₂B), 10.9 (bs, *BMe*). **$^{31}\text{P}\{^1\text{H}\}$ NMR (202.5 MHz, 298 K, C_6D_6) δ :** 5.59 (s, *PPh*₂). **$^{11}\text{B}\{^1\text{H}\}$ NMR (202.5 MHz, 298 K, C_6D_6) δ :** -15.30 (s, *BMe*₂).

$[\text{Ir}(\text{cod})(\mu\text{-Cl})(\text{Me}_2\text{PCH}_2\text{BMe}_2)]$ (1)

A solution of $(\text{Me}_2\text{PCH}_2\text{BMe}_2)_2$ (136.7 mg; 0.553 mmol) in 2 mL of benzene was added to a solution of $[\{\text{IrCl}(\text{cod})\}_2]$ (373.2 mg; 0.553 mmol) in 3 mL of benzene. This mixture was stirred for 12 hours at 65°C . The resulting deep orange-red solution was evaporated to dryness *in vacuo*, affording pure **1** as an orange-red solid (464.5 mg, 93% yield). X-ray quality crystals of **1** were obtained by layering a CH_2Cl_2 solution of **1** with hexanes (1:2 ratio) and cooling to -30°C . **$\text{C}_{13}\text{H}_{26}\text{BClIr}$ (451.80 g mol $^{-1}$):** calcd. C 34.56 %, H 5.80 %; found C 34.39 %, H 5.93 %. **$^1\text{H NMR}$ (600 MHz, 298 K, C_6D_6) δ :** 5.18 (m, 2H, cod *CH*); 2.88 (m, 2H, cod *CH*); 2.07 (m, 2H, cod *CH*₂); 1.95 (m, 2H, cod *CH*₂), 1.53 (m, 4H, cod *CH*₂), 1.36 (d, 2H, $^2J_{\text{P-H}} = 14.5$ Hz, *PCH*₂B); 1.01 (s, 6H, *BMe*); 0.95 (d, 6H, $^2J_{\text{P-H}} = 9.2$ Hz, *PMe*). **$^{13}\text{C}\{^1\text{H}\}$ NMR (150.9 MHz, 298 K, C_6D_6) δ :** 92.0 (d, $^2J_{\text{P-C}} = 14.6$ Hz, cod *CH*); 51.0 (s, cod *C-H*); 34.1 (d, $^3J_{\text{P-C}} = 3.3$ Hz, cod *CH*₂); 30.4 (b.s., *PCH*₂B); 29.3 (d, $^3J_{\text{P-C}} = 2.3$ Hz, cod *CH*₂), 16.2 (b.s., *BMe*); 13.6 (d, $^1J_{\text{P-C}} = 31.5$ Hz, *PMe*). **$^{31}\text{P}\{^1\text{H}\}$ NMR (242.9 MHz, 298 K, C_6D_6) δ :** -3.32 (s) (shoulder/side peak observed at -3.34 ppm due to unknown effect). **$^{11}\text{B}\{^1\text{H}\}$ NMR (192.5 MHz, 298 K, C_6D_6) δ :** 66.3 (s). **$^{31}\text{P}\{^1\text{H}\}$ NMR (242.9 MHz, 298 K, CD_2Cl_2) δ :** -7.74 (s, *PMe*₂), (shoulder on peak at -7.69 ppm) **$^{11}\text{B}\{^1\text{H}\}$ NMR (192.5 MHz, 298 K, CD_2Cl_2) δ :** 75.53 (bs).

Reaction of $[\{\text{RhCl}(\text{cod})\}_2]$ with $(\text{Me}_2\text{PCH}_2\text{BMe}_2)_2$

A solution of $(\text{Me}_2\text{PCH}_2\text{BMe}_2)_2$ (66.0 mg; 0.284 mmol) in 1 mL of benzene was added to a solution of $[\{\text{RhCl}(\text{cod})\}_2]$ (140.2 mg; 0.284 mmol) in 2 mL of benzene. This mixture was stirred for 72 hours at 70°C . The resulting yellow solution was evaporated to dryness *in vacuo* to afford a yellow solid (164.4 mg). This solid was dissolved in a minimum volume of CH_2Cl_2 and cooled to -30°C to afford a mixture of clear colourless crystals and yellow crystals, which were identified by single crystal X-ray diffraction and NMR spectroscopy as $(\text{Me}_2\text{PCH}_2\text{BMe}_2)_2$ and $[\text{Rh}(\text{cod})(\mu\text{-Cl})(\text{Me}_2\text{PCH}_2\text{BMe}_2)]_2 \cdot [\{\text{RhCl}(\text{cod})\}_2]$ ($2 \cdot [\{\text{Rh}(\mu\text{-Cl})(\text{cod})\}_2]$),

respectively. The following NMR data is for the solid formed upon evaporation of the reaction mixture to dryness; * indicates $[\text{Rh}(\text{cod})(\mu\text{-Cl})(\text{Me}_2\text{PCH}_2\text{BMe}_2)]$ (**2**), † indicates $[\{\text{Rh}(\mu\text{-Cl})(\text{cod})\}_2]$, and ‡ indicates free $(\text{Me}_2\text{PCH}_2\text{BMe}_2)_2$. **$^1\text{H NMR}$ (600 MHz, 298 K, C_6D_6) δ :** 5.42 (m, 2H, cod *CH**); 4.31 (m, 1H, cod *CH*†); 3.24 (m, 2H, cod *CH**); 2.09 (m, 3.4 H, cod *CH*₂*†); 1.96 (m, 2H, cod *CH*₂*); 1.70 (m, 2H, cod *CH*₂*); 1.63 (m, 2H, cod *CH*₂*); 1.31 (m, 1.4 H, *PCH*₂B†), 1.16 (d, 2H, $^2J_{\text{P-H}} = 14.4$ Hz, *PCH*₂B*); 1.00 (s, 6H, *BMe*₂*); 0.87 (d, 6H, $^2J_{\text{P-H}} = 9.1$ Hz, *PMe*₂*), 0.73 (d, 1.6H, $^2J_{\text{P-H}} = 9.8$ Hz, *PMe*₂†), 0.48 (bm, 0.6 H, *PCH*₂B†), 0.02 (d, 1.3H, $^3J_{\text{P-H}} = 9.8$ Hz, *BMe*₂†); integrations given relative to one another, as in spectrum. **$^{13}\text{C}\{^1\text{H}\}$ NMR (150.9 MHz, 298 K, C_6D_6) δ :** 103.52 (q, $^2J_{\text{CP}} =$ Hz, cod *CH**); 78.5 (d, $^2J_{\text{P-C}} = 14.0$ Hz, cod *CH*†); 68.3 (d, $^1J_{\text{CP}} = 14.3$ Hz, cod *CH**); 33.3 (s, cod *CH*₂*); 30.9 (s, cod *CH*₂†); 30.8 (bs, cod *CH*₂*); 29.7 (bs, *PCH*₂B*); 28.5 (s cod *CH*₂*); 15.8 (bs, *BMe*₂*); 14.6 (d, $^1J_{\text{P-C}} = 24.9$ Hz, *PMe*₂*); 9.12 (d, $^1J_{\text{P-C}} = 29.9$ Hz, *PMe*₂†). **$^{31}\text{P}\{^1\text{H}\}$ NMR (242.9 MHz, 298 K, C_6D_6) δ :** 11.1 (d, $^1J_{\text{Rh-P}} = 142$ Hz), shoulder/side peak observed at 11.2 ppm (d, $^1J_{\text{Rh-P}} = 142$ Hz) due to unknown effect; -5.94 (q, $^1J_{\text{B-P}} = 55.2$ Hz, *PMe*†). **$^{11}\text{B}\{^1\text{H}\}$ NMR (192.5 MHz, 298 K, C_6D_6) δ :** 48.95 (s, *BMe**); -19.30 (d, $^1J_{\text{P-B}} = 59.2$ Hz *BMe*₂†). **$^{31}\text{P}\{^1\text{H}\}$ NMR (242.9 MHz, 298 K, CD_2Cl_2) δ :** 5.08 (s, $^1J_{\text{Rh-P}} = 143.74$ Hz, *PMe*₂), (shoulder on peak at 5.16 ppm, $^1J_{\text{Rh-P}} = 143.77$ Hz) **$^{11}\text{B}\{^1\text{H}\}$ NMR (192.5 MHz, 298 K, CD_2Cl_2) δ :** 65.15 (bs).

***cis*- $[\text{Pt}(\mu\text{-Cl})_2(\text{Me}_2\text{PCH}_2\text{BMe}_2)_2]$ (3)**

A solution of $(\text{Me}_2\text{PCH}_2\text{BMe}_2)_2$ (46.7 mg; 0.200 mmol) in 1 mL of benzene was added to a suspension of $[\text{PtCl}_2(\text{cod})]$ (75.0 mg; 0.200 mmol) in 2 mL of benzene. This mixture was stirred for 12 hours at 65°C . The resulting pale yellow solution was evaporated to dryness *in vacuo* to afford a very pale yellow solid (76 mg, 76 % yield). Subsequent crystallization from a concentrated solution CH_2Cl_2 layered with hexanes (1:2 ratio) at -30°C afforded pure **3** as X-ray quality crystals which were dried *in vacuo* (recrystallized yield 38.7 mg, 38.7 %). **$\text{C}_{10}\text{H}_{28}\text{B}_2\text{Cl}_2\text{P}_2\text{Pt}$ (497.88 g mol $^{-1}$):** calcd. C 24.12 %, H 5.67 %; found C 24.14 %, H 5.29 %. **$^1\text{H NMR}$ (600 MHz, 298 K, CD_2Cl_2) δ :** 1.76 (d, 6H, $^2J_{\text{P-H}} = 10.4$ Hz, *PMe*); 1.39 (d, 2H, $^2J_{\text{P-H}} = 14.8$ Hz, *PCH*₂B); 0.47 (s, 6H, *BMe*). **$^{13}\text{C}\{^1\text{H}\}$ NMR (150.9 MHz, 298 K, CD_2Cl_2) δ :** 33.03 (bs, *PCH*₂B); 17.63 (d, $^1J_{\text{P-C}} = 41.6$, *PMe*); 13.36 (bs, *BMe*). **$^{31}\text{P}\{^1\text{H}\}$ NMR (242.9 MHz, 298 K, CD_2Cl_2) δ :** -0.69 ($^1J_{\text{Pt-P}} = 3513.8$ Hz). **$^{11}\text{B}\{^1\text{H}\}$ NMR (192.5 MHz, 298 K, CD_2Cl_2) δ :** 37.77 (bs).

$[\text{Ir}(\text{cod})(\mu\text{-Cl})(\text{Ph}_2\text{PCH}_2\text{BMe}_2)]$ (4)

A solution of $(\text{Ph}_2\text{PCH}_2\text{BMe}_2)_2$ (42.8 mg, 0.089 mmol) in 1 mL of CH_2Cl_2 was added to a solution of $[\{\text{IrCl}(\text{cod})\}_2]$ (59.7 mg, 0.089 mmol) in 2 mL of CH_2Cl_2 . The solution turned from red-pink to bright orange over the course of an hour at room temperature. The crude product was isolated as a bright orange powder (96.9 mg, 97% crude yield) after removal of the solvent *in vacuo*. Subsequent recrystallization from a concentrated solution of CH_2Cl_2 layered with hexanes (1:10) at -30°C afforded X-ray quality crystals of **4** ($0.5 \text{ CH}_2\text{Cl}_2$, which were dried *in vacuo* to afford **4** (56 mg, 56% recrystallized yield). **$\text{C}_{23}\text{H}_{30}\text{BClIr}$ (575.94 g mol $^{-1}$):** calcd. C 47.96 %, H 5.25 %; found C 47.69 %, H 5.31 %. **$^1\text{H NMR}$ (600 MHz, 298 K, C_6D_6) δ :** 7.53 (m, 4H, *m-Ph*); 7.04 (m, 6H, *o,p-Ph*); 5.20 (m, 2H, cod-*CH*); 2.83 (m, 2H, cod-*CH*); 2.0–1.9

(m, 4H, cod-CH₂); 1.83 (d, 2H, ²J_{P-H} = 12.7 Hz, PCH₂B); 1.47 (m, 2H, cod-CH₂); 1.34 (m, 2H, cod-CH₂); 0.82 (s, 6H, BMe₂). ¹³C{¹H} NMR (150.9 MHz, 298K, C₆D₆) δ: 135.22 (d, ¹J_{P-C} = 47.1 Hz, *i*-Ph); 133.90 (d, ³J_{P-C} = 10.3 Hz, *m*-Ph); 130.24 (d, ⁴J_{P-C} = 1.94 Hz, *p*-Ph); 128.5 (*o*-Ph, located from 2D NMR); 91.69 (d, ²J_{P-C} = 13.7 Hz, cod-CH); 54.70 (s, cod-CH); 33.46 (d, *J*_{P-C} = 3.28 Hz, cod-CH₂); 29.40 (d, *J*_{P-C} = 1.87 Hz, cod-CH₂); 27.85 (d, ¹J_{P-C} = 21.1 Hz, PCH₂B); 14.44 (s, BMe). ³¹P{¹H} NMR (242.9 MHz, 298K, C₆D₆) δ: 32.39 (s, PPh₂) (shoulder/ side peak observed at 30.12 ppm due to unknown effect). ¹¹B{¹H} NMR (192.5 MHz, 298K, C₆D₆) δ: 45.03 (bs). ³¹P{¹H} NMR (242.9 MHz, 298 K, CD₂Cl₂) δ: 30.09 (s, PPh₂), (shoulder on peak at 30.12 ppm) ¹¹B{¹H} NMR (192.5 MHz, 298 K, CD₂Cl₂) δ: 51.28 (bs).

[Rh(cod)(μ-Cl)(Ph₂PCH₂BMe₂)] (5)

A solution of (Ph₂PCH₂BMe₂)₂ (49.5 mg, 0.103 mmol) in 1 mL of CH₂Cl₂ was added to a solution of [RhCl(cod)]₂ (50.6 mg, 0.103 mmol) in 2 mL of CH₂Cl₂. The solution turned from orange to yellow over the course of an hour at room temperature. The crude product was isolated as a yellow powder (88.2 mg, 88% crude yield) after removal of the solvent *in vacuo*. Layering a concentrated CH₂Cl₂ solution of the crude product with hexanes (1:10 ratio) and cooling to -30°C afforded X-ray quality crystals of 5·CH₂Cl₂, which were dried *in vacuo* to afford **5** (61 mg, 61% recrystallized yield). C₂₃H₃₀BClPRh (486.63 g mol⁻¹): calcd. C 56.77 %, H 6.21 %; found C 57.01 %, H 5.78 %. ¹H NMR (600 MHz, 298K, C₆D₆) δ: 7.58 (m, 4H, *p*-PhP); 7.05 (m, 6H, *o,m*-PhP); 5.48 (s, 2H, cod-CH); 3.18 (m, 2H, cod-CH); 2.08-1.93 (m, 4H, cod-CH₂); 1.85 (d, 2H, ²J_{P-H} = 7.8 Hz, PCH₂B); 1.56 (m, 4H, cod-CH₂); 0.74 (s, 6H, BMe₂). ¹³C{¹H} NMR (150.9 MHz, 298K, C₆D₆) δ: 136.1 (d, *J*_{P-C} = 39.5 Hz, *i*-Ph); 133.6 (d, *J*_{P-C} = 10.7 Hz, *m*-Ph); 130.0 (d, *J*_{P-C} = 2.0 Hz, *p*-Ph); 128.5 (d, *J*_{P-C} = 9.8 Hz, *o*-Ph); 102.3 (dd, *J*_{P-C} = 11.1 Hz, *J*_{P-C} = 6.7 Hz, cod-CH); 71.5 (d, *J*_{P-C} = 14.2 Hz, cod-CH); 32.9 (d, *J*_{P-C} = 2.3 Hz, cod-CH₂); 28.7 (s, cod-CH₂); 28.3 (bs, BCH₂P); 14.69 (bs, BMe). ³¹P{¹H} NMR (242.9 MHz, 298K, C₆D₆) δ: 41.70 (d, ¹J_{Rh-P} = 143.7 Hz). ¹¹B{¹H} NMR (192.5 MHz, 298K, C₆D₆) δ: 34.25 (bs). ³¹P{¹H} NMR (242.9 MHz, 298K, CD₂Cl₂) δ: 40.16 (d, ¹J_{Rh-P} = 144.1 Hz); shoulders on peaks 40.18 (d, ¹J_{Rh-P} = 144.8 Hz). ¹¹B{¹H} NMR (192.5 MHz, 298K, CD₂Cl₂) δ: 39.32 (bs).

[{Rh(coe)(μ-Cl)(Ph₂PCH₂BMe₂)}₂·CH₂Cl₂ (6·CH₂Cl₂)

A solution of (Ph₂PCH₂BMe₂)₂ (47.2 mg, 0.098 mmol) in 1 mL of CH₂Cl₂ was added to a solution of [RhCl(coe)]₂ (70.5 mg, 0.098 mmol) in 2 mL of CH₂Cl₂. The orange-brown solution was allowed to stir for an hour at room temperature. The crude product was isolated as a dark orange solid (103.3 mg, 99% crude yield) after removal of the solvent *in vacuo*. Recrystallization from a concentrated CH₂Cl₂ solution at -30°C afforded X-ray quality crystals of 6·2 CH₂Cl₂, which were dried *in vacuo* to afford 6·CH₂Cl₂ (36.9 mg, 35% recrystallized yield). C₄₆H₆₄B₂Cl₂P₂Rh₂·2CH₂Cl₂ (1062.22 g mol⁻¹): calcd. C 53.14 %, H 6.26 %; found C 53.72 %, H 6.21 %. ¹H NMR (600 MHz, 298K, C₆D₆) δ: 7.72 (m, 4H, *p*-PhP); 7.03 (m, 6H, *o,m*-PhP); 4.27 (s, 1.3H, CH₂Cl₂); 2.60 (m, 4H, coe-CH₂); 2.37 (m, 2H, coe-CH); 2.15 (d, 2H, ²J_{P-H} = 13.5 Hz, PCH₂B); 1.61 (m, 2H, coe-CH₂); 1.25 (m, 6H, coe-CH₂); 1.08 (s, 6H, BMe₂). ¹³C{¹H} NMR (150.9 MHz,

298K, C₆D₆) δ: 135.6 (d, *J*_{P-C} = 44.9 Hz, *i*-Ph); 134.1 (d, *J*_{P-C} = 9.7 Hz, *m*-Ph); 129.8 (s, *p*-Ph), 127.9 (located from 2D NMR data, *o*-Ph); 65.4 (d, ²J_{P-C} = 15.5 Hz, coe-CH); 53.31 (s, CH₂Cl₂); 31.6 (d, ¹J_{P-C} = 22.5 Hz, PCH₂B); 30.8 (s, coe-CH₂); 30.59 (s, coe-CH₂); 26.8 (s, coe-CH₂); 16.6 (s, BMe₂). ³¹P{¹H} NMR (242.9 MHz, 298K, C₆D₆) δ: 54.3 (d, ¹J_{Rh-P} = 191.9 Hz). ¹¹B{¹H} NMR (192.5 MHz, 298K, CD₂Cl₂) δ: 77.62 (bs) (No signal was observed in C₆D₆ due to limited solubility of the compound). ³¹P{¹H} NMR (242.9 MHz, 298K, CD₂Cl₂) δ: 53.45 (¹J_{Rh-P} = 192.1 Hz). ¹¹B{¹H} NMR (192.5 MHz, 298K, CD₂Cl₂) δ: 77.62 (bs).

[RhCl(Ph₂PCH₂BMe₂)₃] (7)

A solution of (Ph₂PCH₂BMe₂)₂ (83.9 mg, 0.35 mmol) in 1 mL of CH₂Cl₂ was added to a solution of [RhCl(coe)]₂ (41.8 mg, 0.058 mmol) in 2 mL of CH₂Cl₂. The orange-red solution was allowed to stir for 30 minutes at room temperature, after which the solvent was promptly removed *in vacuo* to afford a bubbly burgundy oil. This oil was layered with 3 mL of hexanes and sonicated to give crude **7** as a brown powder. Hexanes was decanted, and the brown powder was dried *in vacuo* (51.9 mg, 51.9 % crude yield). The crude product was then recrystallized from a concentrated toluene solution layered with hexanes (1:6 ratio) at -30°C, affording pure **7** as burgundy X-ray quality crystals which were dried *in vacuo* (22.4 mg, 22.5 % recrystallized yield). Note: Compound **7** is not stable for extended periods of time in CH₂Cl₂; some decomposition was observed if **7** was left in CH₂Cl₂ for 4 hours or longer, with significant decomposition after 24 hours at room temperature. C₄₅H₅₄B₃ClP₃Rh (858.62 g mol⁻¹): calcd. C 62.95 %, H 6.34 %; found C 62.56 %, H 6.49 %. In the following NMR data, * refers to the Ph₂PCH₂BMe₂ ligand *trans* to chloride, and † refers to the Ph₂PCH₂BMe₂ ligands that are *trans* to one another. ¹H NMR (500 MHz, 298K, C₆D₆) δ: 7.62 (m, 8H, PhP[†]); 7.28 (m, 4H, PhP^{*}); 6.97 (m, 12H, PhP[†]); 6.79 (m, 2H, PhP^{*}); 6.72 (m, 4H, PhP^{*}); 2.11 (t, 4H, *J*_{P-H} = 4.92 Hz, PCH₂B[†]); 1.53 (d, 2H, ²J_{P-H} = 13.7 Hz, PCH₂B^{*}); 0.93 (s, 6H, BMe₂^{*}); 0.74 (s, 12H, BMe₂[†]). ¹³C{¹H} NMR (125.7 MHz, 298K, C₆D₆) δ: 139.37 (d, ¹J_{P-C} = 42.0 Hz, *i*-Ph^{*}); 138.62 (t, ¹J_{P-C} = 17.8 Hz, *i*-Ph[†]); 134.49 (t, ³J_{P-C} = 6.1 Hz, *m*-Ph[†]); 133.13 (t, ³J_{P-C} = 17.8 Hz, *m*-Ph^{*}); 128.96 (s, *p*-Ph[†]); 128.84 (s, *p*-Ph^{*}); 127.71 (t, ²J_{P-C} = 4.4 Hz, *o*-Ph[†]); 127.44 (d, ²J_{P-C} = 9.6 Hz, *o*-Ph^{*}); 34.88 (located from 2D NMR data, CH₂^{*}); 34.14 (b.s., CH₂[†]); 17.40 (s, BMe₂^{*}); 15.20 (s, BMe₂[†]). ³¹P{¹H} NMR (202.5 MHz, 298K, C₆D₆) δ: 41.64 (dt, ¹J_{Rh-P} = 197.7 Hz, ²J_{P-P} = 38.4 Hz, P^{*}); 36.22 (dd, ¹J_{Rh-P} = 136.2 Hz, ²J_{P-P} = 38.4 Hz, P[†]). ¹¹B{¹H} NMR (160.5 MHz, 298K, C₆D₆) δ: 88.53 (bs, 1B^{*}); 50.83 (bs, 2B[†]). ³¹P{¹H} NMR (242.9 MHz, 298K, CD₂Cl₂) δ: 41.17 (dt, 1P, ¹J_{Rh-P} = 197.5 Hz, ²J_{P-P} = 38.7 Hz), 35.37 (dd, 2P, ¹J_{Rh-P} = 137.16 Hz, ²J_{P-P} = 39.0 Hz). ¹¹B{¹H} NMR (192.5 MHz, 298K, CD₂Cl₂) δ: 84.54 (bs, 1B); 50.72 (bs, 2B).

cis-[Pt(μ-Cl)₂(Ph₂PCH₂BMe₂)₂] (8)

A solution of (Ph₂PCH₂BMe₂)₂ (49.2 mg, 0.102 mmol) in 1 mL of CH₂Cl₂ was added to a solution of [PtCl₂(cod)] (38.3 mg, 0.102 mmol) in 2 mL of CH₂Cl₂. The solution turned from clear and colorless to pale yellow over the course of an hour at room temperature. The crude product was isolated as a very pale yellow powder (72.7 mg, 97% crude yield) after removal of the

solvent *in vacuo*. The product was then recrystallized from a concentrated CH₂Cl₂ solution layered with hexanes (1:10 ratio) at –30°C to yield pure **8** as X-ray quality crystals which were dried *in vacuo* (43.7 mg, 58% recrystallized yield). **C₃₀H₃₆B₂Cl₂P₂Pt (746.16 g mol⁻¹):** calcd. C 48.29 %, H 4.86%; found C 48.39 %, H 4.42 %. **¹H NMR (500 MHz, 298K, CD₂Cl₂) δ:** 7.35 (m, 6H, *P-Ph*); 7.17 (m, 4H, *P-Ph*); 1.82 (d, 2H, ²*J*_{P-H} = 15.1 Hz, *PCH₂B*); 0.09 (s, 6H, *BMe₂*). **¹³C{¹H} NMR (125.8 MHz, 298K, CD₂Cl₂) δ:** 133.79 (m, *m-PPh*); 131.02 (s, *p-PPh*); 129.58 (d, ¹*J*_{P-C} = 64.0 Hz, *i-PPh*); 128.13 (t, ²*J*_{P-C} = 5.5 Hz, *o-PPh*); 34.34 (bd, ¹*J*_{P-C} = 31.3 Hz, *PCH₂B*); 12.74 (s, *BMe₂*). **³¹P{¹H} NMR (202.5 MHz, 298K, CD₂Cl₂) δ:** 24.38 (¹*J*_{Pt-P} = 3725 Hz). **¹¹B{¹H} NMR (192.5 MHz, 298K, CD₂Cl₂) δ:** 36.33 (bs).

cis-[PtMe₂(Ph₂PCH₂BMe₂)₂] (**9**)

A solution of (Ph₂PCH₂BMe₂)₂ (43.5 mg, 0.091 mmol), dissolved in 2 mL of benzene was added to a solution of [PtMe₂(cod)] (30.2 mg, 0.091 mmol) in 2 mL of benzene. The clear and colourless solution was stirred at 70 °C for 12 hours in a sealed flask. Solvent was then removed *in vacuo* to afford a pale yellow resin. Hexanes (3 mL) was added to the resin, and the mixture was sonicated for 10 minutes, which yielded an off-white precipitate, and then the solvent was removed again *in vacuo* (51.9 mg, 81.2 % crude yield). Layering a concentrated CH₂Cl₂ solution of the crude product with hexanes (1:4 ratio) and cooling to –30 °C afforded X-ray quality crystals of **9** (5.6 mg, 8.8 % recrystallized yield), although this sample still contained trace impurities and was insufficiently pure for elemental analysis. **¹H NMR (600 MHz, 298K, C₆D₆) δ:** 7.45 (m, 8H, *m-Ph*); 6.96 (m, 12H, *o,p-Ph*); 2.01 (m, 4H, *PCH₂B*); 1.06 (mm, ²*J*_{Pt-H} = 67.8 Hz, *PtMe*); 0.92 (s, 6H, *BMe₂*). **¹³C{¹H} NMR (150.9 MHz, 298K, C₆D₆) δ:** 137.92 (d, ¹*J*_{P-C} = 40.4 Hz, *i-Ph*); 133.25 (m, *m-Ph*); 129.18 (s, *o-Ph*); 127.95 (located from 2D NMR data, *p-Ph*); 28.71 (b.s. *PCH₂B*); 17.08 (s, *BMe₂*); 8.35 (dd, ¹*J*_{Pt-C} = 101.6 Hz, ²*J*_{P-C} = 7.8 Hz, *PtMe₂*). **³¹P{¹H} NMR (242.9 MHz, 298K, C₆D₆) δ:** 17.57 (¹*J*_{Pt-P} = 1872.8 Hz). **¹¹B{¹H} NMR (192.5 MHz, 298K, C₆D₆) δ:** 83.88 (bs).

DFT Calculations

All calculated structures were fully optimized with the ADF/AMS DFT package (SCM, version 2020.102).⁴⁵ Calculations were conducted in the gas phase with the PBE0 functional,^{46,47} the scalar zeroth-order regular approximation (ZORA)⁴⁸⁻⁵³ for relativistic effects, and Grimme's DFT-D3-BJ dispersion correction^{54,55} (parameterized for PBE). Geometry optimizations were conducted using all-electron triple- ζ basis sets with two polarization functions (TZ2P), fine integration grids (Becke^{56,57} verygood), and stricter-than-default convergence criteria (gradients = 0.0001, step = 0.002; or for {[MCl(cod)]₂}, energy = 1 × 10⁻⁶, gradients = 0.00001, step = 0.0002). Calculations were restricted, and analytical frequency calculations⁵⁸⁻⁶⁰ were carried out to ensure that all geometry optimizations led to an energy minimum (for {[MCl(cod)]₂} (M = Ir or Rh), the energy minima were bent structures with angles of 67 and 49° between the Cl–M–Cl planes, respectively; similar bent minima were obtained using PBE/TZ2P or PBE/QZ4P). Visualization of the computational results was performed using the ADF/AMS-GUI (SCM) or Biovia Discovery Studio Visualizer.

Conflicts of interest

There are no conflicts to declare.

Acknowledgements

D.J.H.E thanks NSERC of Canada for a Discovery Grant. We thank Mengyang Cui for preparing the sample for solid state ¹¹B NMR spectroscopy, and obtaining and processing the solid state ¹¹B NMR spectrum. We also thank Leon Focks and Dr. Kevin Sanders for their advice and assistance processing the solid state NMR data, and Dr. Gillian Goward for facilitating the solid state NMR experiment.

Notes and references

† For compounds **1** and **2**, the ¹¹B NMR chemical shift was at significantly higher frequency in CD₂Cl₂ than in C₆D₆. The same trend was observed for **3**, **4**, **5** and **8**, but to a lesser degree. See Table S1.

‡ The reaction of {[Rh(μ-Cl)(coe)₂]₂} with 2 equiv. of (Ph₂PCH₂BMe₂)₂ afforded a mixture of **6** and **7** accompanied by several new ³¹P NMR signals (doublets at 54.46 and 46.10 ppm, as well as a broad singlet at 9.50 ppm), some of which may correspond to a complex containing two equivalents of the Ph₂PCH₂BMe₂ ligand; see Figure S36.

§ The trigonal plane at the free borane in **7** is approximately perpendicular to the distorted square plane at rhodium, resulting in a Rh–C distance of 3.54–3.55 Å to one of the *B*-methyl groups, perhaps allowing for a weak C–H–Rh agostic interaction; C–H–Rh interactions have also been proposed in [RhCl(PPh₃)₃], involving phenyl group *ortho*-hydrogen atoms.³⁵ One methyl group on each Ph₂PCH₂BMe₂ ligand in **9** is positioned above/below the square plane at platinum, affording Pt–C distances of 3.63 and 3.87 Å.

- 1 K. M. Paskaruk, B. E. Cowie and D. J. H. Emslie, in *Comprehensive Coordination Chemistry III*, ed. E. C. Constable, G. Parkin, L. Que, Jr., Elsevier, 2021, vol. 1, pp. 717.
- 2 G. Bouhadir and D. Bourissou, *Chem. Soc. Rev.*, 2016, **45**, 1065.
- 3 R. T. Baker, J. C. Calabrese, S. A. Westcott and T. B. Marder, *J. Am. Chem. Soc.*, 1995, **117**, 8777.
- 4 A. J. M. Miller, J. A. Labinger and J. E. Bercaw, *Organometallics*, 2010, **29**, 4499.
- 5 B. R. Nichols, N. G. Akhmedov, J. L. Petersen and B. V. Popp, *Dalton Trans.*, 2018, **47**, 8456.
- 6 J. A. Bailey, H. A. Sparkes and P. G. Pringle, *Chem. Eur. J.*, 2015, **21**, 5360.
- 7 D. H. A. Boom, A. W. Ehlers, M. Nieger, M. Devillard, G. Bouhadir, D. Bourissou and J. C. Slootweg, *ACS Omega*, 2018, **3**, 3945.
- 8 S. Pal, N. Kathewad, R. Pant and S. Khan, *Inorg. Chem.*, 2015, **54**, 10172.
- 9 D. H. A. Boom, A. W. Ehlers, M. Nieger and J. C. Slootweg, *Z. Naturforsch. B*, 2017, **72**, 781.
- 10 J. A. Garduno, D. S. Glueck, R. E. Hernandez, J. S. Figueroa and A. L. Rheingold, *Organometallics*, 2022, **41**, 1475.
- 11 R. Jana, O. Blacque, Y. F. Jiang and H. Berke, *Eur. J. Inorg. Chem.*, 2013, 3155.
- 12 R. Jana, S. Chakraborty, O. Blacque and H. Berke, *Eur. J. Inorg. Chem.*, 2013, **2013**, 4574.
- 13 F. Jakle, M. Mattner, T. Priermeier and M. Wagner, *J. Organomet. Chem.*, 1995, **502**, 123.

- 14 K. Paskaruk, D. J. H. Emslie and J. F. Britten, *Dalton Trans.*, 2022, **51**, 15040.
- 15 F.-G. Fontaine and D. Zargarian, *J. Am. Chem. Soc.*, 2004, **126**, 8786.
- 16 M. H. Thibault, J. Boudreau, S. Mathiotte, F. Drouin, O. Sigouin, A. Michaud and F.-G. Fontaine, *Organometallics*, 2007, **26**, 3807.
- 17 J. Boudreau and F.-G. Fontaine, *Organometallics*, 2011, **30**, 511.
- 18 J. Rathke and R. Schaeffer, *Inorganic chemistry.*, 1972, **11**, 1150.
- 19 H. H. Karsch, A. Appelt, F. H. Kohler and G. Muller, *Organometallics*, 1985, **4**, 231.
- 20 A. Reyna-Madrigal, N. Ortiz-Pastrana and M. A. Paz-Sandoval, *J. Organomet. Chem.*, 2019, **886**, 13.
- 21 M. Brym and C. Jones, *Transit. Met. Chem.*, 2003, **28**, 595.
- 22 D. J. H. Emslie, B. E. Cowie, S. R. Oakley, N. L. Huk, H. A. Jenkins, L. E. Harrington and J. F. Britten, *Dalton Trans.*, 2012, **41**, 3523
- 23 S. Buschel, A. K. Jungton, T. Bannenberg, S. Randoll, C. G. Hrib, P. G. Jones and M. Tamm, *Chem. Eur. J.*, 2009, **15**, 2176.
- 24 Y. Y. Zhang, G. W. Yang, R. Xie, L. Yang, B. Li and G. P. Wu, *Angew. Chem. Int. Ed.*, 2020, **59**, 23291.
- 25 M. Sengoden, G. A. Bhat and D. J. Darensbourg, *RSC Adv.*, 2022, **12**, 32440.
- 26 L. H. Toporcer, R. E. Dessy and S. I. E. Green, *Inorg. Chem.*, 1965, **4**, 1649.
- 27 F. Bessac and G. Frenking, *Inorg. Chem.*, 2006, **45**, 6956.
- 28 S. Dutta, S. M. De, S. Bose, E. Mahal and D. Koley, *Eur. J. Inorg. Chem.*, 2020, 638.
- 29 D. M. C. Ould, J. L. Carden, R. Page and R. L. Melen, *Inorg. Chem.*, 2020, **59**, 14891.
- 30 A. Albinati, F. Isaia, W. Kaufmann, C. Sorato and L. M. Venanzi, *Inorg. Chem.*, 1989, **28**, 1112.
- 31 N. E. Schore and B. E. LaBelle, *J. Org. Chem.*, 1981, **46**, 2306.
- 32 M. Weger, R. K. Grottsch, M. G. Knaus, M. M. Giومان, D. C. Mayer, P. J. Altmann, E. Mossou, B. Dittrich, A. Pothig and B. Rieger, *Angew. Chem. Int. Ed.*, 2019, **58**, 9797.
- 33 S. A. Weicker, J. W. Dube and P. J. Ragogna, *Organometallics*, 2013, **32**, 6681.
- 34 R. M. Beesley, C. K. Ingold and J. F. Thorpe, *J. Chem. Soc.*, 1915, **107**, 1080.
- 35 M.J.Bennett and P.B.Donaldson, *Inorg. Chem.*, 1977, **16**, 655.
- 36 V. K. Greenacre, M. B. Ansell, S. M. Roe and I. R. Crossley, *Eur. J. Inorg. Chem.*, 2014, 5053.
- 37 J. Grobe, K. Lutke-Brochtrup, B. Krebs, M. Läge, H.-H. Niemeyer and E.-U. Würthwein, *Z. Naturforsch. B*, 2006, **61**, 882.
- 38 B. J. Burger and J. E. Bercaw, in *Experimental Organometallic Chemistry - A Practicum in Synthesis and Characterization*, American Chemical Society, Washington D.C., 1987, vol. 357, pp. 79.
- 39 J. X. McDermott, J. F. White and G. M. Whitesides, *Journal of the American Chemical Society*, 1976, **98**, 6521.
- 40 E. Costa, P. G. Pringle and M. Ravetz, *Inorg. Synth.*, 1997, **31**, 284.
- 41 L. T. Mika, L. Orha, N. Farkas and I. T. Horváth, *Organometallics*, 2009, **28**, 1593.
- 42 H. H. Karsch and H. Schmidbaur, *Z. Naturforsch. B*, 1977, **32**, 762.
- 43 R. K. Harris, E. D. Becker, S. M. C. De Menezes, R. Goodfellow and P. Granger, *Pure Appl. Chem.*, 2001, **73**, 1795.
- 44 D. Massiot, F. Fayon, M. Capron, I. King, S. Le Calve, B. Alonso, J. O. Durand, B. Bujoli, Z. H. Gan and G. Hoatson, *Magn. Reson. Chem.*, 2002, **40**, 70.
- 45 S. ADF 2020.102, Theoretical Chemistry, Vrije Universiteit, Amsterdam, The Netherlands, <http://www.scm.com>.
- 46 S. Grimme, *J. Comput. Chem.*, 2004, **25**, 1463.
- 47 M. Ernzerhof and G. E. Scuseria, *J. Chem. Phys.*, 1999, **110**, 5029.
- 48 J. P. Perdew, K. Burke and M. Ernzerhof, *Phys. Rev. Lett.*, 1996, **77**, 3865.
- 49 E. van Lenthe, E. J. Baerends and J. G. Snijders, *J. Chem. Phys.*, 1993, **99**, 4597.
- 50 E. van Lenthe, E. J. Baerends and J. G. Snijders, *J. Chem. Phys.*, 1994, **101**, 9783.
- 51 E. van Lenthe, J. G. Snijders and E. J. Baerends, *J. Chem. Phys.*, 1996, **105**, 6505.
- 52 E. van Lenthe, R. van Leeuwen, E. J. Baerends and J. G. Snijders, *Int. J. Quantum Chem.*, 1996, **57**, 281.
- 53 E. van Lenthe, A. Ehlers and E.-J. Baerends, *J. Chem. Phys.*, 1999, **110**, 8943.
- 54 S. Grimme, J. Anthony, S. Ehrlich and H. Krieg, *Journal of Chemical Physics* 2010, **132**, 154104.
- 55 S. Grimme, S. Ehrlich and L. Goerigk, *J. Comput. Chem.*, 2011, **32**, 1456.
- 56 A. D. Becke, *J. Chem. Phys.*, 1988, **88**, 2547.
- 57 M. Franchini, P. H. T. Philipsen and L. Visscher, *J. Comput. Chem.*, 2013, **34**, 1819.
- 58 A. Bérces, R. M. Dickson, L. Y. Fan, H. Jacobsen, D. Swerhone and T. Ziegler, *Comput. Phys. Commun.*, 1997, **100**, 247.
- 59 H. Jacobsen, A. Bérces, D. P. Swerhone and T. Ziegler, *Comput. Phys. Commun.*, 1997, **100**, 263.
- 60 S. K. Wolff, *Int. J. Quantum Chem.*, 2005, **104**, 645.